Title

Spatial transcriptional signatures define margin morphogenesis along the proximal–distal and medio-lateral axes in tomato (Solanum lycopersicum) leaves

Journal

The Plant Cell, 33(1)

ISSN

1040-4651

Authors

Martinez, Ciera C
Li, Siyu
Woodhouse, Margaret R
et al.

Publication Date

2021-03-22

DOI

10.1093/plcell/koaa012

Peer reviewed

doi:10.1093/plcell/koaa012

THE PLANT CELL

THE PLANT CELL 2021: 33: 44–65

Large-Scale Biology

Spatial transcriptional signatures define margin morphogenesis along the proximal–distal and medio-lateral axes in tomato (*Solanum lycopersicum*) leaves

Ciera C. Martinez [1,2,3], Siyu Li [3], Margaret R. Woodhouse [3], Keiko Sugimoto [4] and Neelima R. Sinha [3,*]

1 Department of Molecular and Cellular Biology, University of California at Berkeley, Berkeley, CA 94709
2 Berkeley Institute for Data Science, University of California at Berkeley, Berkeley, CA 94709
3 Department of Plant Biology, University of California at Davis, Davis, CA 95616
4 RIKEN Center for Sustainable Resource Science, Tsurumi, Yokohama, 15 230-0045 Japan

*Author for communication: nrsinha@ucdavis.edu

Conceived and designed the experiments: C.M. and N.S. Performed molecular experiments and plant characterizations: C.M. Plant maintenance and phenotyping of *CR-bop2* lines: S.L. Contributed plant lines, protocols, and/or reagents: N.S., K.S. Performed computational analysis: C.M. Performed read mapping: M.W. Analyzed the data: C.M., N.S., and K.S. Wrote the paper: C.M. and N.S. edited the paper: C.M., N.S., and K.S.
The author responsible for distribution of materials integral to the findings presented in this article in accordance with the policy described in the Instructions for Authors (www.plantcell.org) is Neelima R. Sinha (nrsinha@ucdavis.edu).

Abstract

Leaf morphogenesis involves cell division, expansion, and differentiation in the developing leaf, which take place at different rates and at different positions along the medio-lateral and proximal–distal leaf axes. The gene expression changes that control cell fate along these axes remain elusive due to difficulties in precisely isolating tissues. Here, we combined rigorous early leaf characterization, laser capture microdissection, and transcriptomic sequencing to ask how gene expression patterns regulate early leaf morphogenesis in wild-type tomato (*Solanum lycopersicum*) and the leaf morphogenesis mutant *trifoliate*. We observed transcriptional regulation of cell differentiation along the proximal–distal axis and identified molecular signatures delineating the classically defined marginal meristem/blastozone region during early leaf development. We describe the role of endoreduplication during leaf development, when and where leaf cells first achieve photosynthetic competency, and the regulation of auxin transport and signaling along the leaf axes. Knockout mutants of *BLADE-ON-PETIOLE2* exhibited ectopic shoot apical meristem formation on leaves, highlighting the role of this gene in regulating margin tissue identity. We mapped gene expression signatures in specific leaf domains and evaluated the role of each domain in conferring indeterminacy and permitting blade outgrowth. Finally, we generated a global gene expression atlas of the early developing compound leaf.

Introduction

A major theme in plant development is the reiteration of patterning events, which are influenced by the identity and relative arrangement of neighboring plant parts. The phytomer concept describes reiterated units of the leaf, stem, and axillary bud that make up the aboveground shoot

Received May 14, 2020. Accepted October 23, 2020. Advance access publication December 2, 2020

IN A NUTSHELL

Background: Leaf development involves cell division, expansion, and cellular specialization in specific positions along the middle to margin and top to bottom axes of a leaf. These regions expand and develop at different rates.

Question: We wanted to understand what the differences in development are between the middle and the margin of a leaf. We used a microscope-based method and small lasers to dissect out six tiny regions of a young tomato leaf.

Findings: Using precisely dissected regions of the young leaf, we generated a global gene expression atlas of the early developing tomato leaf. We describe when and where leaf cells first begin photosynthesis. Surprisingly, photosynthetic capability is first seen in the middle regions of the leaf and not the blade. We also describe the role of the plant hormone auxin in various regions of the leaf. We evaluated the role of gene expression in each domain in conferring the ability to continue cell division and permitting blade outgrowth. Knockout mutants of one gene, *BLADE-ON-PETIOLE2,* exhibited shoot apical meristem formation on leaves, highlighting the role of this gene in regulating the balance between cell division and blade outgrowth.

Next steps: Since our gene expression dataset is extremely large, we will test more genes that were identified from the dataset to see the exact way in which they control leaf shape early in development.

(Sussex and Kerk, 2001). Molecular analyses comparing development in various plant species suggest that the reiteration of developmental patterning in plants is defined by the recruitment of a common molecular toolbox, and the dizzying array of leaf architecture found in plants results from variations on a common genetic regulatory program (Blein et al., 2008; Bendahmane and Theres, 2011; Tsukaya, 2014).

The shoot apical meristem (SAM), which is located at the growing tip of the shoot, is a dome-like structure containing reservoirs of continually self-renewing stem cells and is characterized by spatially defined zones. The peripheral zone of the SAM gives rise to most lateral organs, including leaves. Like the SAM, the angiosperm leaf has been historically defined in terms of zones and spatial cell organization. Leaf development begins with periclinal cell divisions on the periphery of the SAM and continues as cells proceed through the specific steps of development beginning with cell division, followed by cell expansion and cell specialization. In many instances, this specialization involves endoreduplication. The timing of these stages varies depending on the cell position on the leaf primordium.

Leaf morphogenesis and patterning occur along three main axes: the abaxial–adaxial, proximal–distal, and medio-lateral axes. Many studies have focused on the importance of the abaxial–adaxial boundary in establishing leaf polarity (Eshed et al., 2001; Kidner and Timmermans, 2007; Moon and Hake, 2011), but less is known about the proximal–distal and medio-lateral axes of the leaf. During the development of many eudicot leaves, including those of *Arabidopsis thaliana* (*A. thaliana*) and *Solanum lycopersicum* (tomato), cells differentiate more rapidly in the distal (top) region than in the proximal (base) region. Along the medio-lateral axis, the differentiation at the margin of a leaf is decelerated relative to the more medial regions (midvein, rachis, petiole). Thus, historically, the leaf margin is of particular interest because it maintains cellular pluripotency longer than the other regions and has even been described as a meristematic region termed the marginal meristem (Avery, 1933; Poethig and Sussex, 1985b) or marginal blastozone (Hagemann and Gleissberg, 1996).

Although the developmental fate, homology, and even the name of the margin region of a leaf have been debated for roughly 100 years, there is general agreement that the process of cell differentiation in this region largely determines final leaf shape (Ori et al., 2007; Efroni et al., 2008; Scarpella and Helariutta, 2010). The regulation and modulation of the margin identity of a leaf are responsible for blade expansion, serrations, lobing, vascular patterning, and new organ initiation, as in the case of leaflet initiation in compound leaves (Scarpella et al., 2010; Bilsborough et al., 2011).

The genetic regulation and coordination of leaf morphogenesis involve distinct changes in gene expression, as revealed by leaf transcriptomic studies in spatially defined regions across the proximal–distal axes of the simple-leaved plant *A. thaliana* (Beemster et al., 2005; Efroni et al., 2008; Andriankaja et al., 2012). These studies revealed the role of endoreduplication (DNA replication without cell division) in the acquisition of leaf morphogenic potential (Andriankaja et al., 2012; Beemster et al., 2005; Efroni et al., 2008). The transcriptional mapping of gene expression changes in *A. thaliana* (Beemster et al., 2005; Efroni et al., 2008; Andriankaja et al., 2012), tomato (Ichihashi et al., 2014), and *Zea mays* (maize; Li et al., 2010) shed light on how patterning by cellular differentiation along the proximal–distal axis is established. However, this information has not yet been precisely mapped at the transcriptome level outside of *A. thaliana* (Tian et al. 2019) with sufficient spatial resolution to define margin and midvein/rachis/petiole transcriptional identity in tomato.

Interestingly, the tomato mutant *trifoliate* (*tf-2*) loses morphogenetic competence during early leaf development and produces only three leaflets: a terminal leaflet and two lateral leaflets subtended by a long petiole (Robinson and Rick, 1954; Naz et al., 2013). The *tf-2* phenotype is caused by a nucleotide deletion resulting in a frameshift in the translated amino acid sequence of an R2R3 MYB transcription factor gene (Solyc05g007870; Naz et al., 2013). Histological and

scanning electron microscopy (SEM) analyses of the *tf-2* mutant revealed that the marginal blastozone region is narrower and has fewer cells, a three-fold increase in epidermal cell size, and faster cell differentiation than the wild-type (Naz et al., 2013). While the application of auxin to the margins of wild-type *S. lycopersicum* leaf primordia causes leaflet initiation (Koenig et al., 2009; Naz et al., 2013), in *tf-2*, the margin is unable to generate leaflets in response to exogenous auxin, indicating that it lacks organogenic competency during early development (Naz et al., 2013). Understanding why this mutant is incapable of initiating more than two lateral leaflets, while wild-type leaves continue to generate an average of ten leaflets at maturity (Naz et al., 2013), could help reveal the mechanisms regulating margin maintenance and identity during complex leaf development.

Here, we used the complex tomato leaf as a model system to study the transcriptional mechanisms directing spatial cell differentiation processes during a key developmental stage in a young leaf, including the establishment of margin identity, proximal–distal patterning, and leaflet initiation. Since a leaf primordium develops at varying rates in a spatially defined manner, different developmental stages can be observed at the same time in a single leaf (Hagemann and Gleissberg, 1996; Ori et al., 2007). We anatomically characterized the earliest developmental stages in tomato and identified leaf age P4 as the stage at which the medio-lateral and proximal–distal axes are first identifiable while also containing multiple stages of leaflet organogenesis. We also characterized the role of endoreduplication in tomato leaf morphogenesis. To map the spatial transcriptional regulation of the P4 leaf using laser capture microdissection, we isolated six highly specific tissues previously unattainable during early tomato leaf development and performed RNA-seq analysis to identify gene expression changes that accompany the establishment of spatial cell differentiation patterning during leaf organogenesis. We also included *tf-2* in our analysis, as *tf-2* lines have early loss of morphogenetic potential in the leaf margin, thus helping us uncover a cluster of genes whose expression differs only in regions that define organogenetic capacity in the margin at the P4 stage. We further validated our results through molecular visualization, providing strong evidence for when and where photosynthesis begins in a leaf. We also used Clustered Regularly Interspaced Short Palindromic Repeats (CRISPR) knockout lines to explore the role of BLADE-ON-PETIOLE2 (BOP2; Solyc10g079460) in margin development. Our approach allowed us to predict multiple gene expression differences that help explain the molecular identity of the classically described, but never transcriptionally defined, marginal meristem/blastozone region and to build a global transcriptome atlas of an early developing compound leaf.

Results

Characterization of the P4 stage of tomato leaf development

The goal of this work was to characterize gene expression changes that occur during tomato leaf morphogenesis. We further focused on the medio-lateral axis in an attempt to identify how the marginal blastozone maintains the potential for leaflet organogenesis and the regulation of cell fate identity. We chose to use the leaf stage primordium 4 (P4), the fourth oldest leaf emerging from the apical meristem (Figure 1, A and B). P4 provides a comprehensive snapshot of tomato leaflet development as it contains three distinct stages of leaflet development. During this stage, the most distal region (destined to become the terminal leaflet) is undergoing early blade expansion, while the most proximal region is undergoing lateral leaflet initiation, and central to these positions is the recently initiated lateral leaflets. All

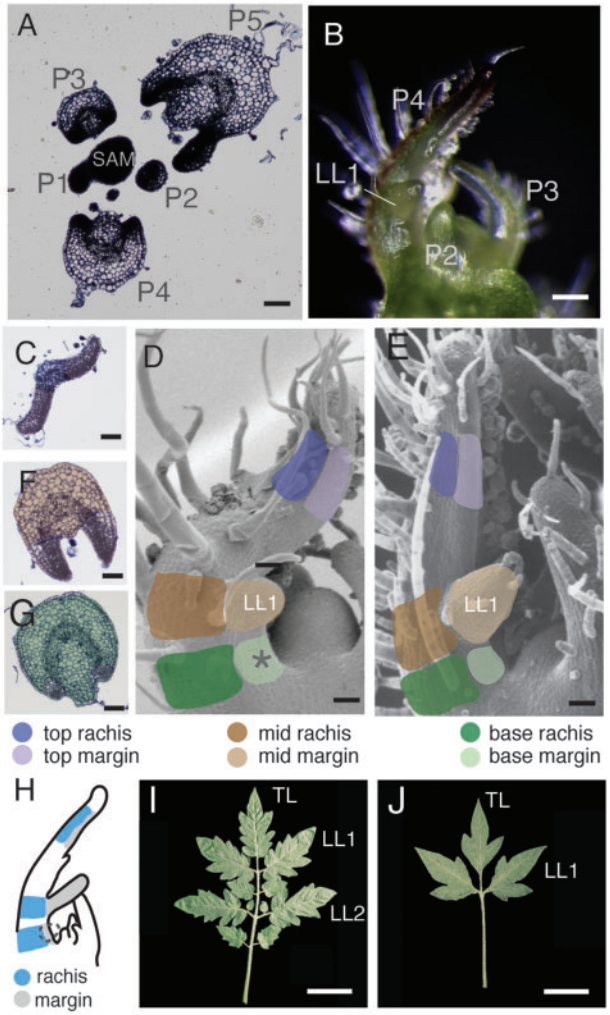

Figure 1 Experimental set-up for sampling *S. lycopersicum* P4 leaves. (A) Transverse section from a wild-type apex showing leaf primordia P1–P5 in relation to the SAM. (B) Image of a wild-type apex during P4 leaf development. Images of transverse sections from the (C) top, (F) middle, and (G) base regions of a wild-type P4 leaf. Colors highlight the separation of the margin (lighter colors) and rachis (darker colors) along the top (purple), middle (brown), and base (green). Schematic diagram of a P4 leaf illustrating the six regions identified in (D) wild-type and (E) *tf-2*. (H) Schematic diagram showing how the margin (gray) and rachis (blue) of a leaf were defined in this study. Images of leaves from wild-type (I) and *tf-2* (J). Scale bars (A–E) = 100 μm and (I) and (J) = 5 mm.

three regions can be defined anatomically, allowing the boundaries along both the medio-lateral and proximal–distal axes to be clearly delineated. With our scope defined, we began our analysis with a systematic survey of tissue differentiation patterns of the P4 leaf using a combination of SEM and histological approaches to establish the cellular context for detailed tissue-specific gene expression analysis.

We defined three distinct regions of the P4 leaf along the proximal–distal axis, which are referred to as the top, middle, and base hereafter (Figure 1, C–G). These three regions can further be divided into two distinct tissues types that define the medio-lateral axis: the margin and the midrib/midvein/rachis, hereafter termed the rachis for brevity (Figure 1, C, G, and F). The most distal region, the top, will ultimately become the terminal leaflet of the mature leaf (Figure 1C). In P4 leaves, the top margin region has already begun to develop lamina tissue (blade) and has not yet developed any tertiary vasculature, but the future midvein in the top contains vascular cells including xylem and phloem (Figure 1C). The middle margin tissue has initiated the first lateral leaflets (henceforth called LL1), the first leaflets to form from the marginal blastozone, and the rachis tissue displays clear vascular bundles and more than four layers of cortex cells (Figure 1F). The most proximal area is the base, where rachis tissue has established vascular bundles (Figure 1, G). Cells in the margins of all three regions along the proximal–distal axis are small and nonvacuolated and have likely undergone little elongation, a characteristic of marginal blastozone tissue (Hagemann and Gleissberg, 1996; Figure 1, C, F, and G). Tomato leaflets initiate in pairs proximal to previous leaflet initiation sites, and therefore, the next leaflets to arise, LLs 2 (LL2) will occur at the base margin region of a P4 leaf (Figure 1D).

To further delineate margin identity, we also characterized *tf-2*, a tomato mutant unable to initiate leaflets past LL1, to compare its margin identity and marginal organogenesis capacity with the wild-type (Figure 1, E and J). The developmental fate of the *tf-2* mutant diverges from that of the wild-type at P4, as the margin is unable to form leaflets after LL1. Therefore, comparing *tf-2* and wild-type allowed us to explore two leaves of comparable developmental age but with different organogenic potential, i.e. different abilities to form leaflets. The anatomical characterization of wild type and *tf-2* revealed precise cell types present across a P4 leaf, serving as a proxy for defining cell differentiation.

Cell division and endoreduplication in the P4 leaf

Previous transcriptomic studies tracing proximal–distal cell division patterning and cellular processing indicated that changes in gene expression are responsible for the regulation of cell division, cell elongation, and endoreduplication during differentiation in developing *A. thaliana* leaves (Donnelly et al., 1999; Beemster et al., 2005; Efroni et al., 2008; Andriankaja et al., 2012). Endoreduplication is thought to be a defining component of *A. thaliana* leaf morphogenesis (Beemster et al., 2005; Gutierrez, 2005), with ploidy levels varying from 2C to 32C (Melaragno et al., 1993; Beemster et al., 2005). Endoreduplication occurs at the onset of leaf differentiation, and elongation occurs after cell proliferation, when cell ploidy levels increase due to successive rounds of DNA replication, often resulting in increased cell size (Kondorosi et al., 2000; Sugimoto-Shirasu and Roberts, 2003; De Veylder et al., 2011). While endoreduplication occurs at rates (256–512C) during tomato fruit development (Bergervoet et al., 1996; Joubès et al., 2000; Cheniclet et al., 2005; Bourdon et al., 2010), where and to what extent endoreduplication occurs during tomato leaf development are currently unknown. Since no reports were available on endoreduplication during tomato leaf development, we carefully characterized cell division and endoreduplication processes at the P4 stage to identify similarities and differences between early leaf development in tomato and Arabidopsis.

To observe where cell division is occurring throughout the P4 leaf, we used 5-ethynyl-29-deoxy-uridine (EdU; Figure 2, A–F), which is incorporated during the S phase of the cell cycle and serves as a proxy to map cell division locations. Along the mediolateral axis, in wild-type and to a lesser extent in *tf-2*, EdU fluorescence was more prominent in the margin compared with rachis tissue (Figure 2, E and F), indicating that the margin tissue is actively undergoing cell division, as expected for marginal blastozone tissue. At the base margin region of wild-type, where LL2 will arise, EdU was incorporated in a cluster (Figure 2E), clearly demonstrating early cell division processes during LL2 initiation. Therefore, during early P4 development, LL2 initiation has already begun, although this is not always obvious based on external views of the leaf (Figure 1, B and D). The *tf-2* mutant did not show clustering of EdU fluorescence in the base margin (Figure 2, E and F), revealing that the cell divisions needed for LL2 initiation have not occurred. In conclusion, cell division across the mediolateral axis in wild-type and *tf-2* reflects similar processes that occur in *A. thaliana* (Donnelly et al., 1999), where cells are actively dividing in the margin. The cell divisions needed for LL2 initiation at P4 have already begun in the wild-type but not in *tf-2*. Interestingly, previous work found *TRIFOLIATE (TF)* expression in the marginal blastozone in initiating wild-type leaflet primordia, in regions that are compromised in a *tf* mutant (Naz et al., 2013). Therefore, the mechanism that restricts LL2 initiation in *tf-2* is likely in place at the P4 stage of development where *TF* spatiotemporal expression could be directly involved.

We used flow cytometry to measure DNA content in tissues from the terminal leaflets of leaves across several developmental ages. We transferred germinated seeds to soil at Day 0 and sampled the oldest leaf on the plant at each time point. Due to the limited availability of tissue from the youngest leaf, we performed flow cytometry of whole terminal leaflet tissue beginning at 8-day old (P6 stage leaf). We detected a combination of 2C and 4C nuclei at all stages examined (Figure 2G). The 4C nuclei were likely G2 nuclei observed following DNA replication and did not reflect the endoreduplication process, although a few 8C nuclei were present at 30 and 60 days, perhaps representing cell type-specific

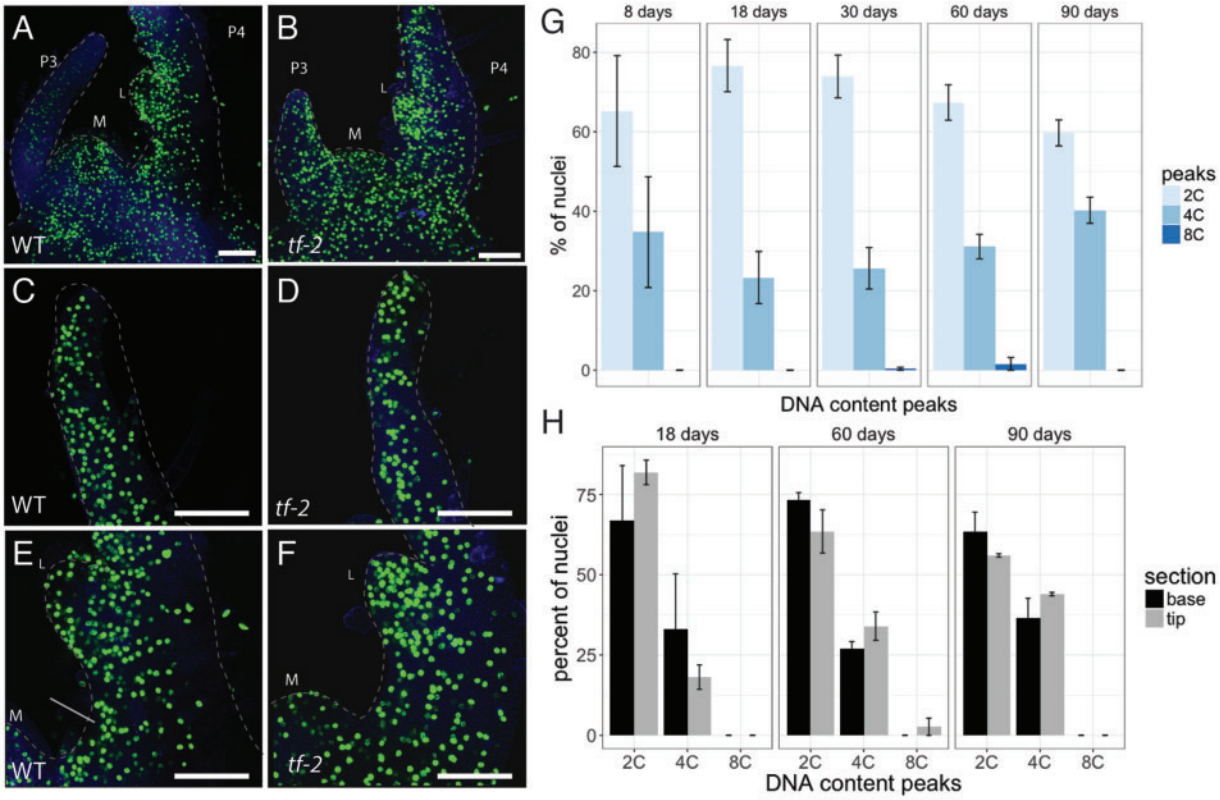

Figure 2 Characterization of the cell cycle using EdU fluorescence and flow cytometry. (A–F) Representative confocal images using EdU fluorescence to detect sites of cell division at the shoot apex of (A, C, and E) wild-type and (B, D, and F) *tf-2* plants. Images in (C and D) show the top region of a P4 leaf, while (E and F) show the middle and base regions of a P4 leaf. Arrow in (E) points to clustering of EdU fluorescence suggesting sites of active cell division needed for leaflet initiation. (G) Bar graph showing DNA content peaks based on flow cytometry of leaf tissue. Tissue was collected from the oldest leaf of the plant at 8–90 days after germination. (H) Bar graph displaying the DNA content peaks from flow cytometry comparing leaf tissue sampled from the base (black) and tip (gray). Error bars show the standard deviation across at least three replicates at each time point. Scale bars = 100 μm.

endocycling (Figure 2G). In *A. thaliana* plants, there is a difference in ploidy level between tip and base cells (Skirycz et al., 2011), but this was not the case in our analysis (Figure 2H). We conclude that endoreduplication is not as pronounced in tomato as in *Arabidopsis* and is likely not a vital aspect of tomato leaf morphogenesis, illustrating the diversity of cellular processes in leaf morphogenetic strategies between species.

Laser capture of six regions of the P4 tomato leaf

Since the P4 leaf is representative of two key developmental processes that define leaf development, i.e., margin versus rachis specification and leaflet initiation and morphogenesis, we analyzed the P4 stage more carefully. We took advantage of our comprehensive anatomical characterizations to generate a map delineating the medio-lateral axis and leaflet organogenesis. We employed laser capture microdissection following explicit rules for tissue collection (Supplemental Figure 1 and Movie 1) on P4 leaves of both wild-type and *tf-2* lines to capture gene expression differences that might explain the morphogenetic differences in the margins of *tf-2* plants. Specifically, we sectioned tomato apices transversely to isolate the same six subregions in both wild-type and *tf-2*, including the (1) top margin blastozone region (top margin), (2) top rachis, (3) middle margin, (4) middle rachis, (5) base margin, and (6) base rachis (Figure 1, C–G and Supplemental Movie 1). We attempted to collect enough tissue for seven replicates per sample, but due to the fragility of RNA at such a small tissue size, a few replicates did not pass quality control and were lost during various steps in the pipeline, resulting in a total of 3–6 biological replicates per region. We collected tissue from 6 to 8 apices per biological replicate to obtain a minimum of 2 ng of RNA per replicate. The number of cuts needed to achieve minimum RNA levels varied depending on sample and tissue density, and the total tissue area collected also varied among samples (Supplemental Figure 2, B and D). The isolated mRNA from the collected tissues was further amplified and prepared for Illumina sequencing (see Methods section). Each replicate resulted in an average of 4.9 million sequencing reads (Supplemental Figure 2, A and C). To assess the overall similarity between samples, we visualized gene expression using Multidimensional Scaling for each of the six subregions per genotype. Tissue types in each genotype generally clustered together in multidimensional space (Supplemental Figure 2A) and we observed an additional separation of margin and rachis tissue regions (Supplemental Figure 2C). The expression patterns from all

tomato genes can be visualized using an interactive electronic fluorescent pictographic (eFP) (http://bar.utoronto.ca/efp_tomato/cgi-bin/efpWeb.cgi?dataSource=Tomato_Meristem).

Differential gene expression between wild-type margin and rachis tissue along the proximal–distal axis reveals signatures of morphogenetic states during early leaf development

Identifying genes that are differentially regulated in margin versus rachis tissue in each region would shed light on gene expression patterning along the medio-lateral axis. To explore the differences between margin and rachis tissue in the three regions along the proximal–distal axis, we performed pairwise differential gene expression analysis of wild-type samples comparing the margin and rachis in each region (top, middle, base) separately (Supplemental Data Set 1) using edgeR (Robinson et al., 2010). We then performed gene ontology (GO) enrichment analysis of the significantly upregulated genes in these samples (Benjamini-Hochberg (BH)-adjusted $P < 0.05$; Supplemental Data Set 2). More upregulated genes in the margin region, which has historically been considered to proceed at a slower rate through the morphogenetic stages, were enriched in GO terms associated with cell processes that occur during early morphogenesis compared with rachis tissue. For example, when we looked for differentially expressed genes between the margin and rachis tissue in the top region, we identified 603 genes that were upregulated in the margin (Supplemental Figure 3A). These genes were enriched in GO terms that likely reflecting cell groh processes (Figure 3, A and Supplemental Data Set 2). Conversely, upregulated genes in the top rachis region were enriched in GO terms reflecting the cell specialization stage of morphogenesis, including terms related to transport, photosynthesis, sugar biosynthesis, and carbohydrate metabolism (Figure 3, A–C and Supplemental Data Set 2).

A comparison of genes expressed in the margin and rachis in the most proximal region (the base) revealed 1,722 genes that were upregulated in the rachis, which were enriched for GO terms related to cell wall biogenesis, transporter activity, and metabolic processing. In contrast, only 94 differentially expressed genes were upregulated in the margin tissue at the base (Supplemental Figure 3A). These upregulated genes in the margin were enriched for GO terms related to transcription factor activity and DNA binding (Supplemental Data Set 2). The types of genes that were differentially expressed between the margin and rachis also appeared to reflect that stage of morphogenesis of each region and perhaps the distal-to-proximal wave of differentiation as summarized in Figure 3, B and C. The upregulated genes in the top and middle margin regions were enriched in GO terms describing active RNA, DNA, and chromatin processing, whereas those in the base were enriched in GO terms similar to those in the rachis. The active processing of RNA, DNA, and chromatin are key gene expression signatures of cell division and expansion. The base region of the P4 leaf is still in these middle stages of morphogenesis and just beginning to start secondary cell wall biosynthesis and to become specialized for sucrose transport activity (Figure 3, A; Supplemental Data Set 2).

Taken together, the enriched GO terms of the differentially expressed genes describe different stages of morphogenesis, pointing to two trajectories of development along the leaf: development along the proximal–distal axis and the medio-lateral axis (Figure 3, B and C). Cells that have achieved specialized photosynthetic functions, leaf development, and sugar transport define the final morphogenetic stages. Margin regions undergoing active cell division are defined by chromatin assembly and DNA processing (replication, integration, and recombination), which are required for proper cell cycle progression, while the most highly meristematic tissue in the margin region at the base is defined by only transcriptional activity and transcription factor and DNA binding (Figure 3, A–C). Thus, the P4 tomato leaf represents a complex mixture of developmentally distinct regions that cannot be defined solely along the proximal–distal or medio-lateral axes.

Modeling gene expression differences across the medio-lateral axis predicts that photosynthetic activity first occurs in the rachis

Differential gene expression analysis in each region along the proximal–distal axis revealed specific genes and enriched GO terms that are unique to the top, middle, or base of the leaf. Next, we tried to identify gene activity that defines rachis and margin identity across the entire P4 leaf primordium regardless of position on the longitudinal axis. To address this issue, we performed differential gene expression analysis across the margin and rachis tissue and adjusted for variability between the proximal–distal axis by employing an additive linear model using the top, middle, and base identities as a blocking factor in our experimental design using EdgeR (Robinson et al., 2010). In the wild-type, across the entire proximal–distal axis, 1,089 genes were significantly upregulated in the rachis and 188 genes were significantly upregulated in the margin (Figure 4, A; Supplemental Data Set 3). GO enrichment analysis of these upregulated genes revealed 24 enriched GO terms in the rachis (Supplemental Data Set 4). These terms were categorized into eight major categories: sugar biosynthesis and transport, metabolism (carbohydrate and glucose), transmembrane transport, leaf development, photosynthesis/light harvesting, catalytic activity, cell wall organization, and response to light (Figure 4B). These categories reflect the activities of genes that were upregulated in the rachis compared with the margin across the entire proximal–distal axis. These results suggest that the rachis region of a P4 leaf has many specialized tissue types and may already be physiologically active.

Verifying photosynthetic gene expression patterns

Of the gene expression patterns described above, the most prominent pattern revealed by both pairwise and modeled

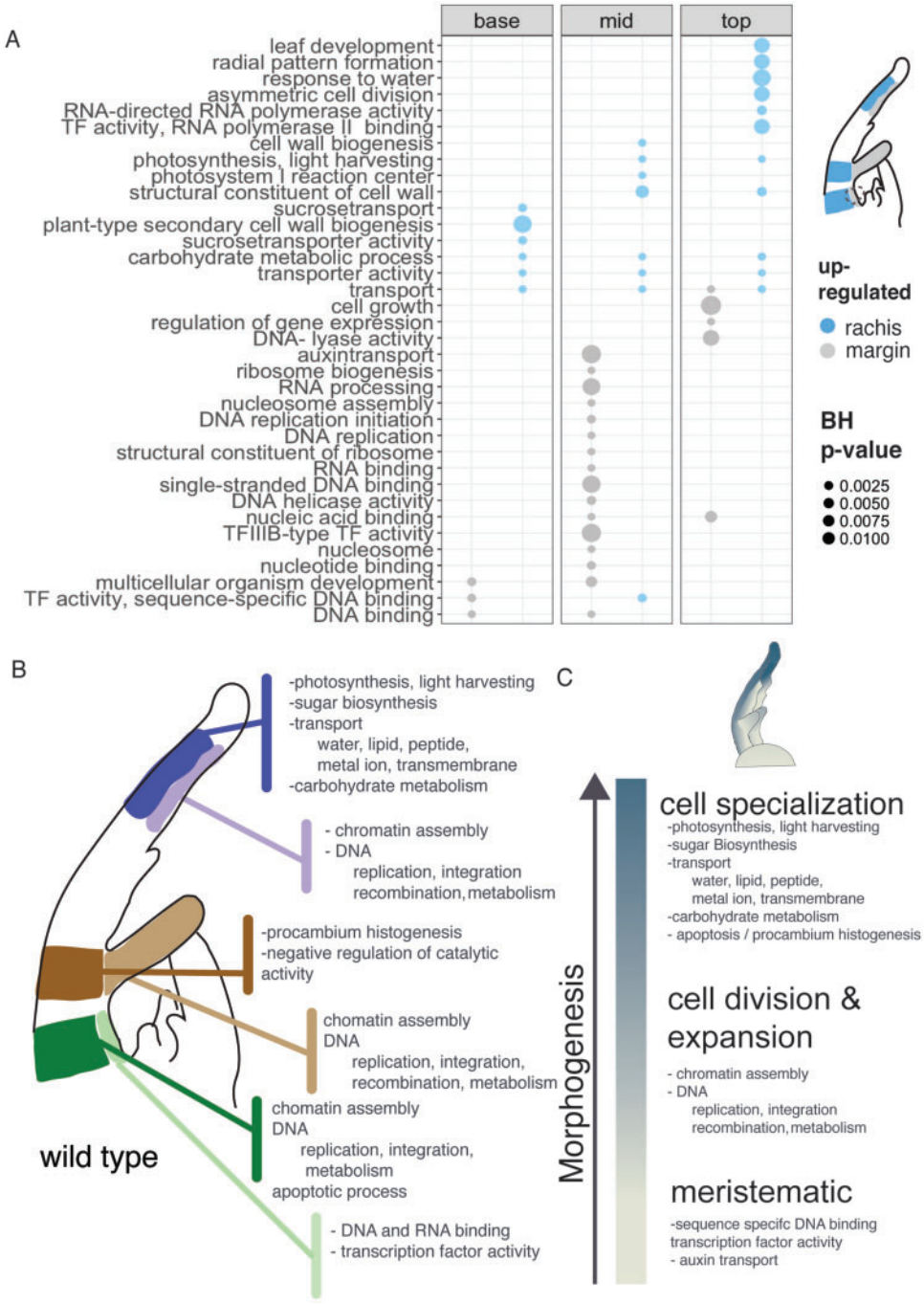

Figure 3 Pairwise differential gene expression between the rachis and margin in each region along the proximal–distal axis in a wild-type P4 leaf. (A) Graph summarizing representative enriched GO terms describing the significantly upregulated genes in each region (top, mid, and base) from differential gene expression analyses performed on wild-type plants (see Methods section). Point size represents Benjamini–Hochberg (BH) corrected P-values in margin (gray) and rachis (blue) tissue. (B) Schematic diagram summarizing enriched GO terms of differentially upregulated genes in each region of the P4 leaf. Colors highlight the separation of the margin (lighter colors) and rachis (darker colors) along the top (purple), middle (brown), and base (green). (C) Schematic diagram showing GO categories that help define each morphogenetic state along the leaf.

differential expression analyses was the persistent presence of genes associated with GO terms related to photosynthetic processes; these genes were upregulated in the rachis compared with margin tissues (Figures 3 and 4). While the upregulation of genes involved in cell wall development, leaf development, and transport might be expected in the rachis, a region of the leaf that acts as a connective corridor to the rest of the plant, we were surprised to find upregulation of so many genes defined by GO terms related to photosynthesis. As noted in the pairwise differential gene expression analysis described above, the most abundant enriched GO terms for upregulated genes in the rachis were related to

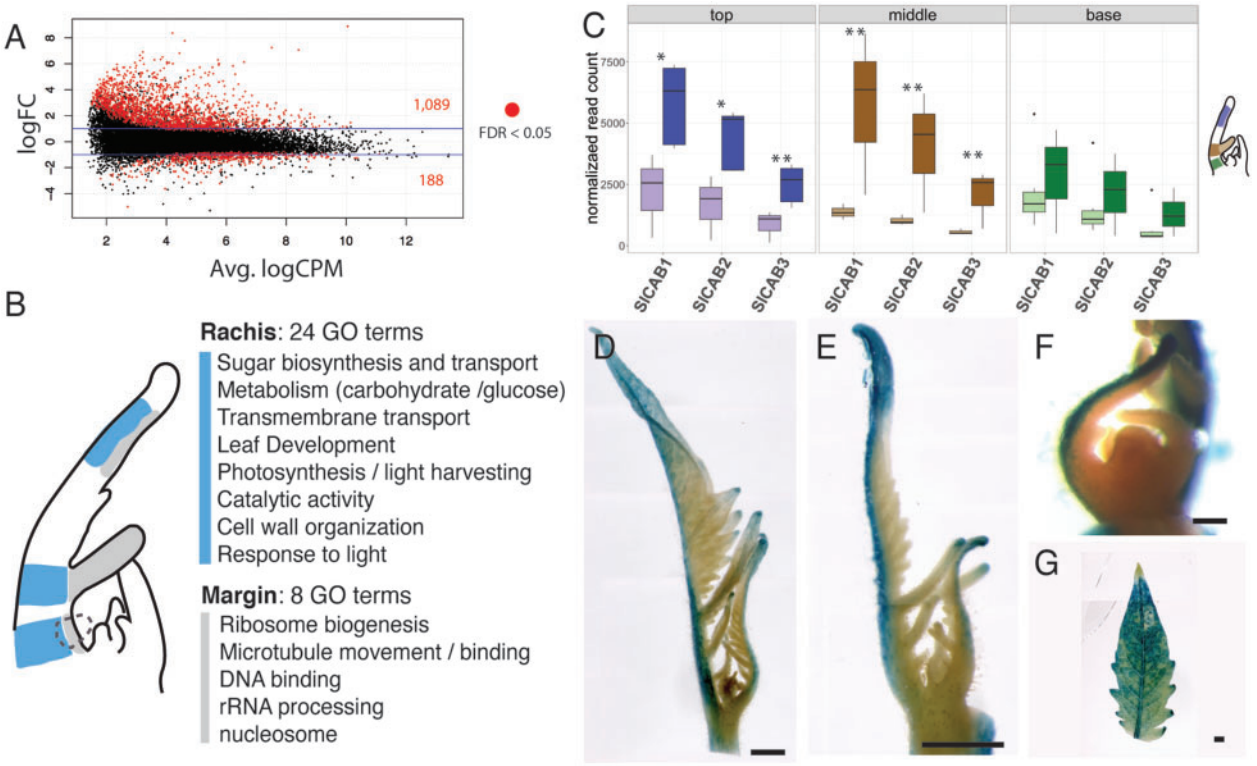

Figure 4 Differential gene expression between the margin and rachis in a wild-type P4 leaf and CAB binding gene activity in the rachis compared with margin tissue during early leaf development. (A) Results of differential gene expression analysis in the wild-type showing average Log c.p.m. over log fold change (logFC) values. The number of significant (based on false-discovery rate <0.05) differentially regulated genes (red) between margin and rachis tissue is shown. (B) Summary of GO terms describing upregulated genes in each tissue, showing that rachis (blue) tissue is predominantly described by GO terms related to cell specialization compared with margin tissue (gray). (C) Normalized read count for CAB binding genes in tomato (*SlCAB*). Colors highlight the separation of the margin (lighter colors) and rachis (darker colors) along the top (purple), middle (brown), and base (green). (D–G) pCAB:GUS expression showing photosynthetic activity during leaf development in tomato. pCAB:GUS is localized to the rachis of P4-P6 leaflets, illustrating differential regulation of *CAB* expression along the medio-lateral axis during early leaf development. pCAB:GUS is nearly ubiquitous in (G) P8 terminal leaflet. $^*p < 0.005$ for significantly upregulated genes in rachis tissue compared with the margin based on modeled differential expression analysis. Scale bars (D, E, and G) = 1 mm, (F) = 100 μm.

sugar biosynthesis and photosynthesis, indicating that the rachis region likely has functioning photosynthetic machinery before it is acquired by the P4 margin, which is destined to become the blade, the primary photosynthetic tissue of the leaf. Since little is known about when photosynthesis first begins in a developing leaf, and no previous studies have described photosynthesis specifically in the rachis, we attempted to verify the notion that the rachis is a photosynthetic force during early leaf development.

To verify the photosynthetic signature repeatedly found to be upregulated in rachis compared with margin tissue, we searched for photosynthetic genes in our data set that showed significant differential expression between the rachis and margin in each longitudinal region. We identified three *Light Harvesting Chlorophyll A-B binding* (*CAB*) genes (Solyc03g005760 [*SlCAB1*], Solyc03g005770 [*SlCAB2*], and Solyc03g005780 [*SlCAB3*]) with significantly upregulated expression in the rachis regions compared with the margin (Figure 4C; Supplemental Data Set 1). CAB proteins balance excitation energy between Photosystems I and II during photosynthesis (Liu and Shen, 2004) and are important components of photosynthesis.

In an attempt to verify the gene expression differences identified in our experimental setup and visualize when and where photosynthetic activity begins in a leaf primordium, we constructed a transgenic line expressing a representative *CAB* gene promoter attached to the β-glucuronidase (GUS) reporter (*pCAB1:CAB1:GUS*; Mitra et al., 2009; Tindamanyire et al., 2013). In the expanded leaflets of P8 leaves, *pCAB:CAB1:GUS* expression was nearly ubiquitous across the entire blade (Figure 4, D). At this age, the leaf had the anatomy of a fully functional photosynthetic organ. As predicted from our gene expression analysis, in younger leaf primordia, we found a clear *pCAB:CAB1:GUS* signal localized predominantly in the rachis region along the proximal–distal axis in P4-P7 leaves (Figure 4, E and F). The *pCAB:CAB1:GUS* signal spread to the distal tips of newly established leaflets and lobes after P4 and continued to spread to the margin tissue as development proceeded until the entire leaf showed expression (Figure 4, D–G).

Since pCAB:CAB1:GUS is predominantly expressed in the rachis region during early development, we suggest that the rachis is the first region in a developing leaf to function photosynthetically, as predicted in our RNA-seq analysis. The

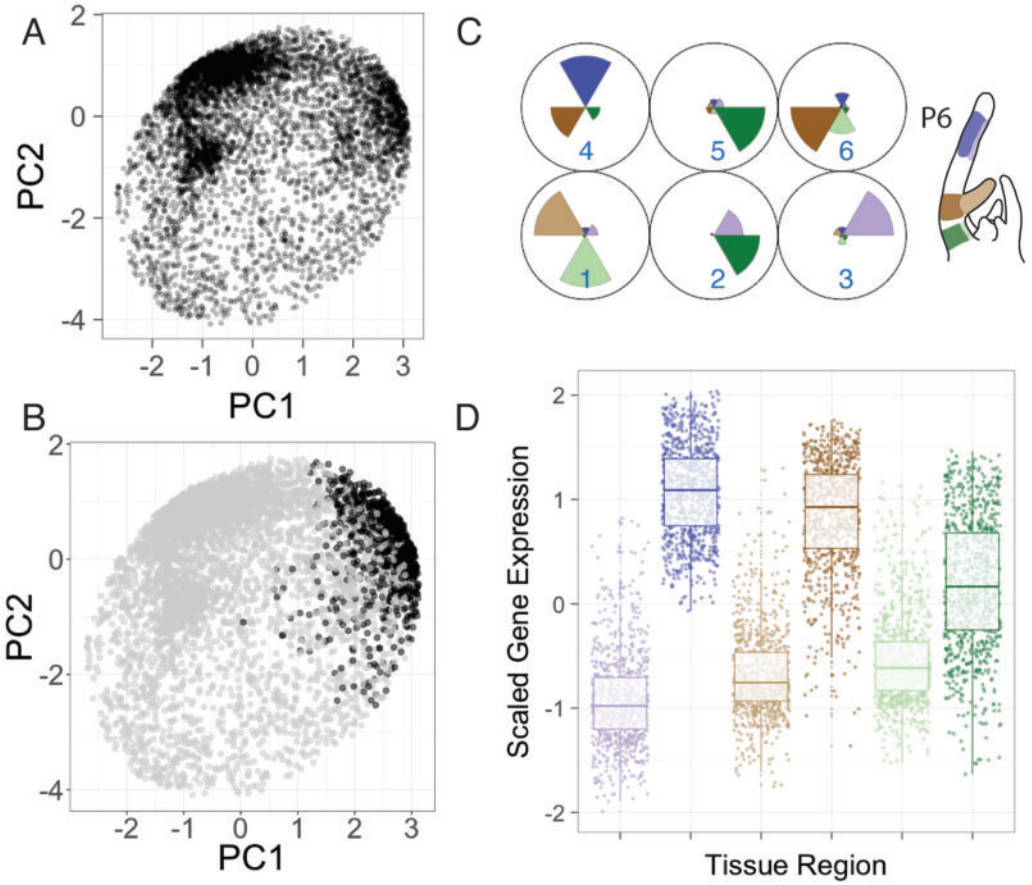

Figure 5 Top clusters identified by SOM analysis define each tissue region based on upregulated genes. (A) Plotting of wild-type gene expression observed in the top 25% of genes based on coefficient of variation in the PC space. (B) Projection of SOM cluster 4 onto the PC space explains one of the main clusters in the PC space, (C) Codebook vector of a 2 × 3 SOM analysis showing the top six clusters, (D) gene expression patterns of Cluster 4 across the six tissue types. (C) and (D) Colors highlight the margin (lighter colors) and rachis (darker colors) along the top (purple), middle (brown), and base (green).

enrichment of photosynthetic genes in the rachis provides evidence that during a very early developmental stage (P4), the rachis region does not simply function as a conduit for nutrients and water transport, but it also functions in photosynthesis and sugar production.

Self-organizing maps identify specific groups of genes that share similar expression patterns

To refine our results and identify groups of genes sharing similar co-expression patterns that may be too complex to define by differential expression analysis alone, we used self-organizing map (SOM) analysis to cluster genes based on gene expression patterns across the six tissue groups. SOM (Tamayo et al., 1999) begins by randomly assigning a gene to a cluster. Other genes are subsequently assigned to clusters based on similar expression patterns via a reiterative process informed by previous cluster assignments. This clustering method allows genes to be grouped based on specific expression patterns shared across different tissues, allowing genes to be classified into smaller groups than those generated by differential expression analysis alone. SOM analysis also allowed us to survey the most prominent types of gene expression patterns found in our data.

To focus on the most variable genes across tissues, we selected the top 25% of genes with the highest coefficients of variation, resulting in a data set of 6,582 unique genes (Supplemental Data Set 5). We used principal component (PC) analysis to visualize groups of genes and found that the first four PCs explained 31.9, 26.2, 19.0, and 13.5% of the amount of variation in the data set, respectively (Supplemental Figure 5A). Looking at the expression of these genes in the PC space revealed distinct clusters of genes with related expression patterns (Figure 5A), which show us that there is clearly identifiable similar clusters of gene expression.

We started with a small SOM cluster map of six, to identify the gene expression patterns that define the main clusters in PC space, to view the most prominent gene expression patterns in our data, and further verify what was found in our DE and GO enrichment work (Supplemental Data Set 6). To identify the most common gene expression patterns that describe the data, SOM analysis was initially limited to six clusters. One of these clusters, Cluster 4

(with 1,090 genes), defines a clear separation of margin and rachis tissues, which again reinforces our finding that the expression levels of many genes differ depending on where the sampled tissue is localized along the medio-lateral axis (margin versus rachis). This cluster is enriched in genes defined by carbohydrate metabolic processes, hydrolase activity, protein dimerization, membrane, transporter activity, and photosynthesis and light harvesting (Supplemental Figure 5 and Data Set 7). These findings mirror the results obtained by differential gene expression analysis and reflect the overall abundance and diversity of genes upregulated in the rachis and downregulated in margin, comprising the largest signal in our data set. These findings likely reflect the specialization that occurs in tissues as the rachis develops an identity distinct from the margin.

Auxin transport and regulation as a defining feature of margin identity

To refine our analysis of gene expression patterns to genes that direct margin identity, we generated a larger clustering map. We used this approach to obtain a smaller subset of genes than could be obtained by differential gene expression analysis or SOM clustering using a smaller number of clusters. We were especially interested in identifying specific types of gene expression patterns that defined the medio-lateral axis; in this case, we looked for groups of genes that were preferentially up or downregulated in the margin compared with the rachis. We specified 36 clusters in a 6 × 6 hexagonal topology, forcing interactions between multiple tissue types (Figure 6, A; Supplemental Figure 5). We surveyed the gene expression patterns of each of the 36 clusters (Supplemental Data Set 8) and identified Clusters 10 (n = 108) and 11 (n = 112), which describe a group of genes that were upregulated in the margin and downregulated in the rachis in stage P4 wild-type plants (Figure 6, B and C). While over half of these genes (57.2%; 126/220) have no known function, many of the remaining genes are known to be involved in leaf margin identity (Table 1). Interestingly, Clusters 10 and 11 also contained genes related to auxin transport, biosynthesis, and regulation (*YUC4*, *PIN1*, *AUX2-11*) and genes (*ARGONAUTE7*/Solyc01g010970) known to interact with auxin response factors (Yifhar et al. 2012).

Guided by the gene expression data in the wild-type, and the results suggesting that auxin might play a role leaflet initiation in the base margin region, we wanted to see if auxin transport differences in *tf-2* could explain the striking feature of loss of meristematic potential in the basal margin of this mutant. To look specifically at the differences in auxin transport between *tf-2* and wild-type and to verify the differences in *SlPIN1* gene expression found between the wild type and *tf-2*, we crossed a fluorescently labeled *pPIN1:PIN1-GFP* line (*PIN1:GFP*; Benková et al., 2003; Koenig et al., 2009) with *tf-2* to visualize differences in PIN1 localization and expression in P4 leaves. In the wild-type, PIN1:GFP was present along the entire margin region of a P4 leaf, with the strongest signal present at the site of the newly established LL1 (Figure 7, A and B). In *tf-2*, there was an overall decrease in fluorescent signal along the margin of a P4 leaf. Also, *tf-2* had a noticeable decrease in PIN1:GFP fluorescent signal in the base margin region (Figure 7, C and D). In addition, we visualized auxin presence using the auxin-inducible promoter DR5:Venus (Bayer et al., 2009). As observed previously (Shani et al., 2010; Martinez et al., 2016), in the wild-type, DR5:Venus was expressed at the site of leaflet initiation as a sharp wedge-shaped focus region (Figure 7, E and F). In contrast, in *tf-2*, there was a DR5:Venus focus region, but it was diffuse and located in the upper layers of the margin (Figure 7, G and H). These results support the hypothesis that while *tf-2* is capable of forming auxin foci, it is incapable of maintaining proper auxin foci and canalization processes, as evidenced by the reduced *PIN1* expression in the basal margin region of the *tf-2* P4

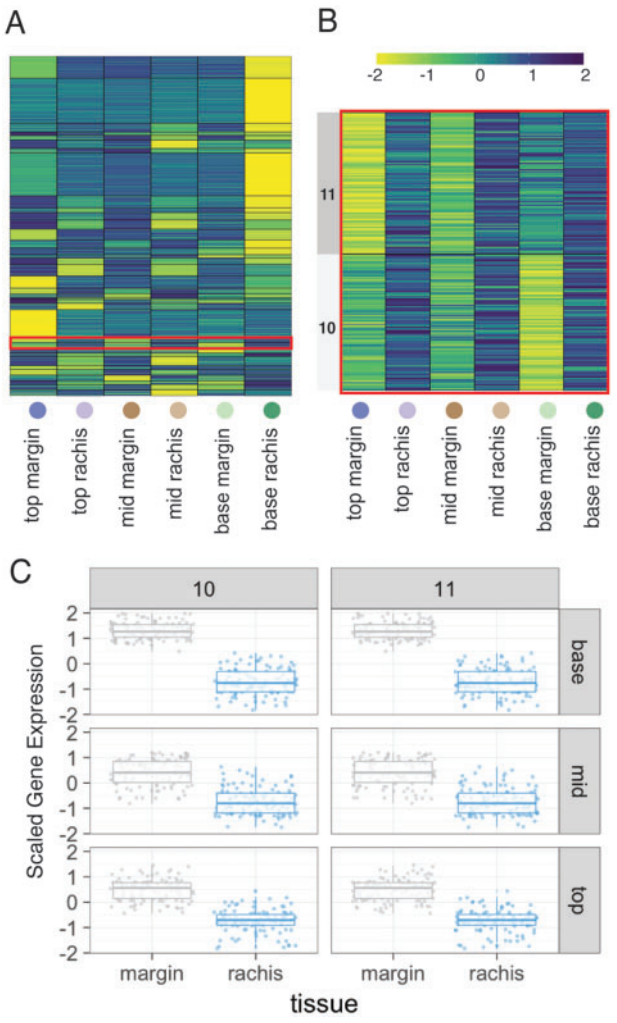

Figure 6 Large SOM map describes a small gene cluster that defines margin identity. (A) Heatmap representing the gene expression patterns of the 36 gene clusters. The red box highlights clusters 10 and 11. (B) Heatmap of clusters 10 and 11, with genes that are upregulated in the margin and downregulated in the rachis. (C) Boxplot showing the gene expression patterns of clusters 10 and 11. See Supplemental Figure 5 for full heatmap of all 36 clusters.

Table 1 Leaf development genes which are upregulated in margin tissue compared with rachis tissue

ITAG	logFC	logCPM	*P*-value	FDR	symbol	Gene_name
Solyc01g010970	−3.060	3.655	7.94E−11	5.29E−08	AGO7	Encodes ARGONAUTE7, a member of the ARGONAUTE family, characterized by the presence of PAZ and PIWI domains. Involved in the regulation of developmental timing
Solyc01g058030	−2.579	4.765	4.03E−09	1.17E−06	ATGA2OX4	Encodes a gibberellin 2-oxidase. AtGA2OX4 expression is responsive to cytokinin and KNOX activities
Solyc03g093310	−2.553	5.232	4.49E−09	1.26E−06	NA	F-box family protein; similar to F-box family protein [*Arabidopsis thaliana*] (TAIR:AT5G51380.1)
Solyc06g062900	−2.056	5.309	1.37E−06	1.62E−04	EER4	transcription initiation factor IID (TFIID) subunit A family protein; similar to TAFII58 (tata-associated factor II 58) [*Arabidopsis thaliana*] (TAIR:AT3G10070.1)
Solyc03g044300	−1.949	2.412	6.37E−05	3.73E−03	AP2	Encodes a floral homeotic gene, a member of the AP2/EREBP (ethylene responsive element binding protein) class of transcription factors and is involved in the specification of floral organ identity, establishment of floral meristem identity, suppression of floral meristem indeterminacy, and development of the ovule and seed coat
Solyc06g069430	−1.878	4.123	1.32E−05	9.92E−04	AGL8	MADS box gene negatively regulated by APETALA1
Solyc11g069500	−1.850	6.114	1.01E−05	7.94E−04	ARF10	Involved in root cap cell differentiation
Solyc10g080880	−1.714	5.112	4.88E−05	3.00E−03	ATPIN1	Encodes a putative auxin efflux carrier involved in shoot and root development. It is involved in the maintenance of embryonic auxin gradients
Solyc08g080120	−1.671	5.772	6.33E−05	3.72E−03	IXR11	Encodes a homeodomain transcription factor of the Knotted family. May be involved in secondary cell wall biosynthesis. Mutants have moderately irregular xylem development
Solyc01g007870	−1.668	4.731	8.47E−05	4.70E−03	NA	Similar to unknown protein [Arabidopsis thaliana] (TAIR:AT5G06270.1)
Solyc06g066340	−1.594	4.125	2.07E−04	9.44E−03	KAN2	Encodes a member of the KANADI family of putative transcription factors. Together with KAN1, this gene appears to be involved in the development of the carpel and the outer integument of the ovule
Solyc06g059730	−1.482	3.109	9.27E−04	3.04E−02	PIN6	Rate-limiting factor in saturable efflux of auxins. PINs are directly involved of in catalyzing cellular auxin efflux
Solyc08g048430	−1.458	4.183	6.33E−04	2.30E−02	NA	F-box family protein; similar to F-box family protein [Arabidopsis thaliana] (TAIR:AT4G18380.1)
Solyc08g023460	−1.416	5.178	6.79E−04	2.41E−02	NA	LEM3 (ligand-effect modulator 3) family protein / CDC50 family protein; [Arabidopsis thaliana] (TAIR:AT3G12740.1)
Solyc06g069790	−1.310	7.245	1.37E−03	4.14E−02	NA	Gibberellin-responsive protein, putative; similar to GASA4 (GAST1 PROTEIN HOMOLOG 4) [Arabidopsis thaliana] (TAIR:AT5G15230.1); similar to Gip1-like protein [*Populus tomentosa*] (GB:AAV84588.1); contains InterPro domain Gibberellin regulated protein; (InterPro:IPR003854)
Solyc11g069190	1.292	7.985	1.56E−03	4.54E−02	ARF4	Encodes a member of the ARF family of transcription factors which mediate auxin responses. ARF4 appears to have redundant function with ETT(ARF3) in specifying abaxial cell identity
Solyc01g097290	1.317	5.626	1.34E−03	4.04E−02	IAA16	Early auxin-induced (IAA16)
Solyc03g063140	1.351	2.980	1.62E−03	4.67E−02	AS2	required for formation of a symmetric flat leaf lamina, encodes a member of a family of proteins characterized by cysteine repeats and a leucine zipper; involved in KNOX gene regulation. Acts together with ASL1 in proximal–distal symmetry determination
Solyc07g008180	1.415	4.468	7.44E−04	2.59E−02	YAB5	plant-specific transcription factor YABBY family protein; Identical to Axial regulator YABBY5 (YAB5) [Arabidopsis Thaliana] (GB:Q8GW46;GB:O48725); similar to YAB2 (YABBY 2), transcription factor [Arabidopsis thaliana] (TAIR:AT1G08465.1)
Solyc05g007180	1.499	6.766	2.64E−04	1.13E−02	ATHB13	Encodes a homeodomain leucine zipper class I (HD-Zip I) protein

(continued)

Table 1 Continued

ITAG	logFC	logCPM	*P*-value	FDR	symbol	Gene_name
Solyc09g082830	1.500	7.957	2.54E−04	1.10E−02	AGO10	Translation initiation factor. Required to establish the central-peripheral organization of the embryo apex. Along with WUS and CLV genes, controls the relative organization of central zone and peripheral zone cells in meristems
Solyc06g049050	1.961	3.880	6.17E−06	5.35E−04	ATEXP8	Member of Alpha-Expansin Gene Family. Naming convention from the Expansin Working Group (Kende et al., 2004, Plant Mol Bio). Involved in the formation of nematode-induced syncytia in roots of Arabidopsis thaliana

Using SOM clustering we identified 36 clusters defined by their gene expression patterns across 6 tissue types in wild-type. Clusters 10 and 11 showed a similar expression pattern of upregulation in the margin tissue (top, middle, and base) compared with rachis tissue (top, middle, and base). This table is the leaf development genes from those gene lists.

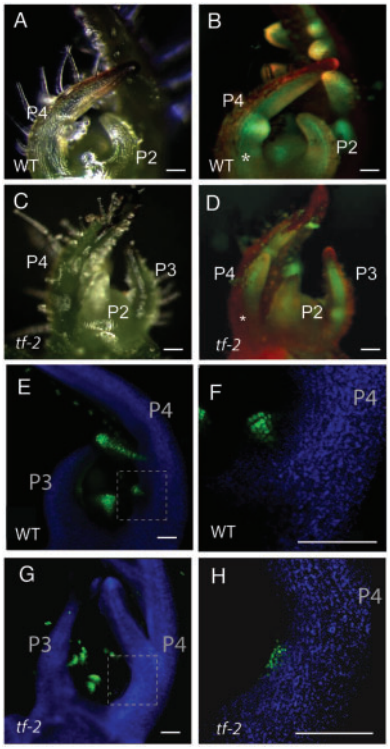

Figure 7 Auxin visualization during leaflet initiation in wild type and *tf-2*. (A–D) Microscope images of apices from (A) and (B) wild-type and (C) and (D) *tf-2*. (B) and (D) Fluorescence signals of PIN1:GFP (green) and chlorophyll autofluorescence (red) asterisk marks the base marginal blastozone region. (B) shows clear PIN1:GFP signal in wild-type along the entire margin of the P4 leaf, while in (D), *tf-2* has lost signal in the base marginal blastozone region. (E–H) DR5:Venus signal (green) observed by confocal microscopy. (E and F) Wild-type plant apices. (G and H) *tf-2* plants apices (F) and (H) close up on the site of leaflet initiation of the base margin region of P4 leaves. Scale bars = 100 μm.

leaf. The transcriptomic results and auxin visualization experiments suggest that misregulated auxin transport and biosynthesis, and specifically *SlPIN1* misregulation, are important contributors to the *tf-2* phenotype and that these processes are vital regulators of margin organogenesis.

Differences in gene expression patterns between the wild-type and *tf-2* help define the loss of basal meristematic potential in *tf-2* leaves

We included *tf-2* in this study because it has the intriguing phenotype of being unable to form new leaflets after the first two LL1 leaflets. At the P4 stage, *tf-2* has already lost the organogenetic ability to initiate new leaflets. As revealed by our auxin transport visualization analysis, *tf-2* appears to receive a leaflet initiation signal, as it is capable of forming auxin foci (Figure 7H), but the tissue is unable to initiate leaflet organs. We examined our data to determine whether gene expression differences could explain the loss of meristematic competency in *tf-2*. We performed differential gene expression analysis of only *tf-2* reads. There were fewer differentially expressed genes between the margin and rachis in the top and base regions of this mutant compared with the wild-type (Supplemental Figure 3, A and Data Set 1). However, *tf-2* followed similar gene expression trends to the wild-type when margin and rachis identity were compared. The margin was more enriched in genes related to cell division and cell expansion, while the rachis was enriched in genes related to specialization, including water transport, metabolic processes, photosynthesis, and leaf development; however, these differences were mostly apparent in the base region of the *tf-2* mutant (Supplemental Figure 3, B and C, Dataset 10). The main difference between wild-type and the *tf-2* mutant was a reduction in upregulated differentially expressed genes in the rachis region compared with the margin in top, middle, and base regions (Supplemental Figure 3A). It should be noted that while wild-type and *tf-2* were similar morphologically at the P4 stage, the *tf-2* mutant appeared to be further along in the morphogenesis process in all regions (top, middle, and base), a feature described by Naz et al. (2013). This overall difference in the two genotypes should be taken into account at the morphological level, and, as evidenced by our transcriptional analysis, at the molecular level. In the margin of *tf-2*, we examined the differentially expressed genes between the rachis and margin and found many genes related to leaf development.

SlBOP2 function in regulating margin and rachis identity

Taking into account the overall differences between these two genotypes, we were interested in understanding why *tf-2* is unable to initiate lateral leaflets beyond LL1. Could transcriptional differences explain the loss of morphogenic capacity in *tf-2*? To address this issue, we combined both genotypes and used a generalized linear model (glmQLFTest in edgeR) in which we defined each genotype as a group and therefore could compare the top, middle, and base regions of the two genotypes. When we compared the base margin region between *tf-2* and the wild type (Figure 1A), only 23 genes were differentially expressed: all were downregulated in the wild-type compared with *tf-2* (Table 2). We focused on the 12 genes that were functionally annotated and noticed that *SlBOP2* was significantly upregulated in the margin of *tf-2* compared with the wild-type (Figure 8B).

We explored the role of *SlBOP2* in regulating margin and rachis tissue identity by phenotyping CRISPR/Cas9 gene edited loss-of-function *SlBOP2* mutants (*CR-slbop2*; Xu et al., 2016) with a focus on leaf phenotypes. Surprisingly, in *CR-slbop2* plants, we observed ectopic meristems on mature leaves when plants were approximately two months old. The ectopic meristems occurred along the adaxial rachis of mature leaves at the bases of primary leaflets (Figure 8, C–E). These ectopic SAM structures did not persist as the leave aged, appearing to undergo tissue death ~3 weeks after appearing on the rachis (Supplemental Figure 6A) and only rarely did they generate complex leaf-like organs (Supplemental Figure 6C). Loss of function of *SlBOP2* also resulted in increased leaf complexity (Supplemental Figure 6B), as reported previously in these mutants (Xu et al., 2016) and in *SlBOP2* knockdown lines (Ichihashi et al., 2014). Since TF is a known transcription factor, we checked for TF binding site motifs in the 3-kb upstream region of *BOP2* and found one TF binding site (Figure 8F). Taken together, these findings indicate that *SlBOP2* functions in determining margin meristematic identity along the rachis of the leaf and the possibility that *SlBOP2* functions via the direct binding of TF to its upstream regulatory region, although more validation is needed to verify this interaction.

Discussion

Characterizing leaf development mechanisms along the proximal–distal and medio-lateral axes

The overall goal of this work was to gain a better understanding of the processes that regulate leaf morphogenesis along the medio-lateral axis in an early developing compound leaf. As endoreduplication is a defining component of *A. thaliana* leaf development (Beemster et al., 2005; Gutierrez, 2005), we chose to explore the contribution of cell cycling in tomato leaf development. Our flow cytometry experiment shows low ploidy levels, with a majority of nuclei at 2C and 4C, with only small traces of 8C, even in mature leaves (Figure 2, G and H). These results suggest endoreduplication is not a major component of leaf morphogenesis in tomato. Tomato leaves have a similar pattern to that observed in closely related species *Solanum tuberosum* leaves (potato; Pijnacker et al., 1989) and the low ploidy numbers found in many monocots—which do not endocycle and grow by ploidy independent mechanisms. It is possible that ploidy differences between cell types, such as trichomes, mesophyll, or epidermal cells, could obscure endocycling signatures that may be present in tomato and occurring in tissue-specific ways, as we sampled whole leaf tissue. One of the reasons tomato leaves might differ from *A. thaliana* is trichome morphology; *A. thaliana* trichomes are single celled and reach an average ploidy level of 32C (Hülskamp et al., 1994), while tomato trichomes are multicellular, suggesting cell division as a strategy of enlarging instead of endoreduplication. Overall, we suggest that the mode of groh of leaves seems to be species dependent, but more work measuring ploidy in a tissue specific way is needed to understand the contribution of ploidy at the cellular level.

Based on our anatomical analysis, we chose six unique regions in the P4 leaf (Figure 1, C–F). We analyzed differential gene expression between margin and rachis tissue in the top, middle, and base regions and identified signature patterns of gene regulation along the proximal–distal (tip-base) axis (Figure 3) that help define leaf morphogenesis in the early tomato leaf primordium. Separating the rachis from the marginal blastozone region at three different points along the proximal–distal axis allowed us to determine whether development proceeds uniformly along the proximal–distal axis or if the leaf has a mosaic of developmental states in each segment along the proximal–distal axis. The further along in morphogenesis a region was, the more diverse the GO categories of genes that were upregulated in the region, likely because the last stage of leaf morphogenesis, cell specialization, had occurred. After summarizing the enriched GO terms in each of the three regions along the proximal–distal axis, patterns of developmentally distinct processes were identified in the rachis regions compared with other tissues (Figure 3). The margin regions, classically defined as the marginal blastozone or marginal meristem, retain the potential to divide and differentiate and also exhibit a basipetal gradient of gene expression changes of differentiation from the tip to the base of the leaf. Thus, this analysis suggests that defining leaf development or capturing gene expression in the entire primordium, or even in regions along the proximal–distal axis, does not provide an accurate picture of developmental patterns in a leaf. Further dissecting these events at cellular resolution should help define these patterns even more accurately.

Photosynthetic capability in the rachis as a regulator of medio-lateral differentiation

To further define rachis and margin identity, we fitted an additive model that adjusts differential gene expression comparisons based on baseline differences that occur between the margin and rachis. We then performed differential gene

Table 2 List of differentially expressed genes from comparing *tf-2* and wild-type base margin tissue

ITAG	logFC	logCPM	*F*	*P*-value	FDR	Gene_name
Solyc02g065250	−2.015	4.676	34.169	8.95E−06	1.76E−02	Esterase, putative; similar to ACL (ACETONE-CYANOHYDRIN LYASE), hydrolase [Arabidopsis thaliana] (TAIR:AT2G23600.1)
Solyc02g077940	−1.586	4.128	39.370	3.43E−06	1.00E−02	(Not Available)NA
Solyc02g091910	−2.669	4.631	37.889	4.47E−06	1.18E−02	NA
Solyc03g111770	−1.544	4.169	32.999	1.13E−05	1.76E−02	Similar to unknown protein [Arabidopsis thaliana] (TAIR:AT5G14390.1)
Solyc04g074700	−1.975	4.010	49.375	6.77E−07	2.43E−03	NA
Solyc05g007870	−3.017	6.247	54.483	3.23E−07	1.70E−03	NA
Solyc05g009270	−2.896	3.837	48.802	7.38E−07	2.43E−03	Involved in wax biosynthesis; required for elongation of C24 very-long-chain fatty acids
Solyc05g014000	−2.224	3.662	28.683	2.74E−05	3.61E−02	Pectate lyase family protein; Identical to Probable pectate lyase 5 precursor
Solyc05g018125	−3.070	3.551	27.696	3.40E−05	4.12E−02	NA
Solyc06g005980	−1.815	4.876	35.734	6.65E−06	1.46E−02	ASA1 encodes the alpha subunit of anthranilate synthase, which catalyzes the rate-limiting step of tryptophan synthesis. ASA1 is induced by ethylene, and forms a link between ethylene signaling and auxin synthesis in roots
Solyc06g050315	−3.700	6.954	69.504	4.78E−08	4.20E−04	NA
Solyc06g051750	−2.491	4.399	33.108	1.10E−05	1.76E−02	Encodes a member of the CP90A family
Solyc06g062670	−2.734	3.575	52.530	4.26E−07	1.87E−03	NA
Solyc06g069460	−3.121	3.742	63.518	9.82E−08	6.46E−04	NA
Solyc06g074630	−2.874	4.409	33.839	9.55E−06	1.76E−02	Encodes a beta-mannan synthase based on in vitro enzyme assays from heterologously expressed protein
Solyc07g055210	−2.325	5.911	32.946	1.14E−05	1.76E−02	ASPARTATE AMINOTRANSFERASE 1
Solyc08g075870	−1.515	4.690	27.432	3.61E−05	4.13E−02	ERD3 (EARLY-RESPONSIVE TO DEHYDRATION 3); similar to dehydration-responsive protein, putative [Arabidopsis thaliana] (TAIR:AT1G31850.2)
Solyc09g014400	−1.946	5.329	27.638	3.45E−05	4.12E−02	NA
Solyc09g014530	−4.439	2.414	36.298	5.98E−06	1.43E−02	NA
Solyc09g061890	−3.087	1.677	32.379	1.27E−05	1.86E−02	Pectate lyase family protein; Identical to Probable pectate lyase 15 precursor
Solyc10g079460	−3.374	3.970	92.395	4.50E−09	5.92E−05	Encodes a cytoplasmic and nuclear-localized NPR1 like protein with BTB/POZ Interacts with BOP1 and appears to be genetically redundant with BOP1.bop1/bop2 double mutants have longer leaves, often with leaflets on the petiole, and asymmetric flowers with extra organs
Solyc11g011570	−1.716	2.906	29.675	2.22E−05	3.08E−02	NA
Solyc11g013430	−5.435	6.606	191.750	6.38E−12	1.68E−07	Encodes the Arabidopsis homologue of yeast SNF5 and represents a conserved subunit of plant SWI/SNF complexes

Using a generalized linear model (glmQLFTest in edgeR), we defined each genotype as a group and made contrasts between the two genotypes at each of the top, middle, and base regions. When we compared the base margin region between *tf-2* and wild–type, we found only 23 genes that were differentially expressed and all of them were downregulated in wild-type compared with *tf-2*.

expression analysis to reveal gene expression trends that define margin and rachis tissue regardless of the position on the proximal–distal axis. The most prevalent, though unexpected, gene expression signature we observed was the enrichment of genes associated with photosynthesis in the rachis, which we found by both differential expression analysis (Figures 3, 7) and cluster analysis (Figure 5). Since little is known about when photosynthetic capacity is acquired during early leaf morphogenesis, we further verified photosynthesis activity using a CAB:GUS reporter (Figure 4, C–G).

This analysis suggested that photosynthetic activity is acquired as early as P4 and is not uniformly distributed along the proximal–distal and medio-lateral axes.

When viewed in the context of cell differentiation processes along each axis, it is not surprising that specialized functions are first acquired in regions that mature earliest, although the function of photosynthesis has been traditionally assigned to the blade. What are the developmental consequences of sugar biosynthesis in the rachis during early leaf organogenesis? Could the rachis be the source of morphogenic signaling towards the more immature base along the proximal–distal axis and along the medio-lateral axis to the margin? Multiple studies in *A. thaliana* identified thousands of genes that respond to changes in sugar levels by modifying transcript abundance (Price et al., 2004; Bläsing et al., 2005; Osuna et al., 2007; Usadel et al., 2008). These

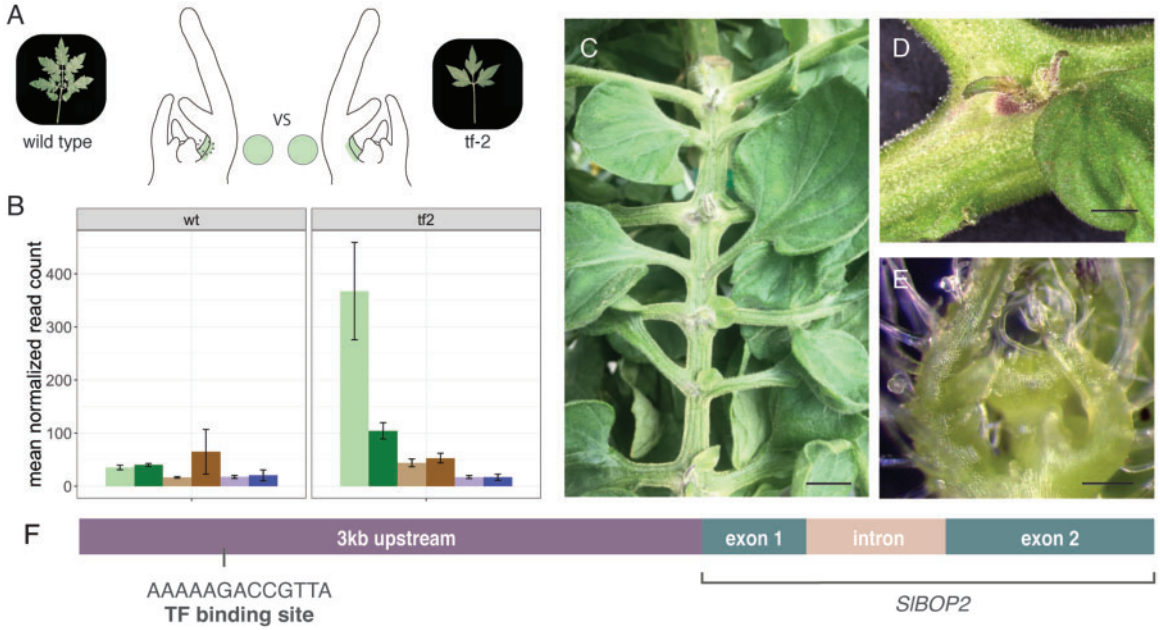

Figure 8 Differential gene expression analysis in base margin tissue between -type and *tf-2* reveals BOP2 as a regulator that suppresses meristematic identity. (A) Schematic illustrating the regions (base margin) compared between wild-type and *tf-2* using modeled differential gene expression analysis. (B) Bar graph illustrating the expression patterns of *SlBOP2* across all six tissue types between wild-type and *tf-2*, showing how *SlBOP2* is upregulated in the base margin only in *tf-2*. Colors highlight the separation of the margin (lighter colors) and rachis (darker colors) along the top (purple), middle (brown), and base (green). (C–E) *SlBOP2* CRISPR knockout line (*CR-slbop2*), which displays ectopic shoot apical meristems along the rachis of complex leaves. (F) *SlBOP2* genomic region. Black line shows the *TF-2* binding site 3kb upstream of *SlBOP2*. Scale bars (C) = 10 mm, (D) = 2 mm, and (E) = 0.2 mm.

studies suggest that the main photosynthetic product, sugar, functions as a signal for plant development and growth. Considering the suggestion that photosynthetic activity and sucrose might function as signaling molecules to help regulate cell differentiation and leaf morphology (Wind et al., 2010; Lastdrager et al., 2014), we propose a potential functional role for the rachis region during early leaf morphogenesis: as a signaling center for cell differentiation.

In the P4 primordium under study, while the rachis has acquired specialized functions, the margin is actively dividing, a process that relies on cell cycle progression. The cyclin genes *CYCD2* and *CYCD3*, encoding critical regulators of the cell cycle, are upregulated in response to sugar (Riou-Khamlichi et al., 2000). Interestingly, sucrose has also been shown to influence auxin levels (Lilley et al., 2012; Sairanen et al., 2012), transport, and signal transduction (Stokes et al., 2013), and metabolism (Ljung, 2013). Moreover, sugar accumulation is spatiotemporally regulated in meristematic tissue in both the shoot and root apical meristem (Francis and Halford, 2006). Is the development of photosynthetic capacity in the rachis a cause or a consequence of its early differentiation? Do the acquisition of photosynthetic capability and the production of sugars represent a global mechanism for signaling quiescent regions to progress into the cell division phase? More work exploring photosynthesis, sugar transport, hormone regulation, and gene expression should help uncover a possible role for the rachis in regulating morphogenetic processes during early leaf organogenesis.

The presence of auxin as a defining feature of organogenic potential in margin tissue

PIN1-directed auxin transport is an important regulator of leaf development (Reinhardt et al., 2003; Heisler et al., 2005; Hay and Tsiantis, 2006; Scarpella et al., 2006; Kawamura et al., 2010; Scarpella and Helariutta, 2010) and leaflet initiation (Koenig et al., 2009). A common mechanism unites PIN1-directed development during leaf organogenesis across the systems studied: PIN1 directs auxin along the epidermal layer to sites of convergence on the meristem and transports the auxin subepidermally into the internal layers (Scarpella et al., 2010). *PIN1* can be split into two highly supported sister clades: *PIN1* and *Sister of PIN1* (*SoPIN1*) (Bennett et al., 2014; O'Connor et al., 2014; Abraham Juárez et al., 2015). The *SoPIN1* and *PIN1* clades might have disparate but complementary functions in auxin transport during organ initiation, where SoPIN1 mainly functions in epidermal auxin flux to establish organ initiation sites and PIN1 functions in the transport of auxin inward (O'Connor et al., 2014; Abraham Juárez et al., 2015; Martinez et al., 2016). Tomato has one gene in the *PIN1* clade (*SlPIN1*) and two genes in the *SoPIN1* clade (*SlSoPIN1a* [Solyc10g078370] and *SlSoPIN1b* [Solyc10g080880]) (Nishio et al., 2010; Pattison and Catalá, 2012; Martinez et al., 2016). The current findings suggest that in *tf-2*, *SlPIN1* is downregulated at the region of leaflet initiation compared with the wild-type. Using *PIN1:GFP* as a reporter, we observed a lack of fluorescence in the base marginal blastozone region of *tf-2* (Figure 7, C–G). Using

DR5:VENUS as a reporter, we observed the diffuse localization of auxin in the base margin region of *tf-2* apices. Interestingly, even with external auxin application, *tf-2* is not capable of leaflet initiation (Naz et al., 2013), suggesting that the ability to direct auxin inwards using PIN1, and not auxin accumulation itself, may be compromised in this mutant. It remains to be seen whether a common theme for organ formation will emerge in organisms in which the *PIN1* clade has diverged into two groups. Based on our findings about the marginal blastozone region in *tf-2*, we suggest that in addition to the creation of auxin foci, the drainage of auxin into internal leaf layers might also be required for leaflet initiation. Analysis of higher-order mutants in the larger *PIN1* clade should help resolve this issue.

Organogenic potential of the margin and homology of the leaf margin and the SAM

In the current study, we were especially interested in obtaining a genetic understanding of the loss of organogenetic potential in the base margin of *tf-2*. We specifically looked for the transcriptional differences that explain the loss of organogenetic potential in *tf-2* compared with the wild-type, specifically in the margin base region. This led us to a small list of 23 differentially expressed genes including *SlBOP2* (Figure 8 and Table 2). Characterization of the *CR-bop2* line (Figure 8) revealed ectopic SAM production along the adaxial rachis at the bases of primary leaflets of the complex leaf. This finding supports the notion that the suppression of meristematic identity by BLADE-ON-PETIOLE (BOP) family members is important during leaf morphogenesis. BOP1 was first introduced as a suppressor of lamina differentiation on the petioles of simple Arabidopsis leaves (Ha et al., 2003, 2004) that limits meristematic cell activity, as the *bop1* mutant displays ectopic meristematic cells beyond the boundary between the base of the blade and petiole (Ha et al., 2003, 2004). Further work using *SlBOP* knockdown and knockout tomato lines demonstrated that SlBOP2 suppresses organogenetic potential (Supplemental Figure 6; Ichihashi et al., 2014; Xu et al., 2016), as lines with reduced or absent *SlBOP* function showed increased leaflet organ initiation/leaf complexity. BOPs interact with transcription factors to regulate floral identity, including the interaction of BOP with PERIANTHIA (PAN) in Arabidopsis (Hepworth and Pautot, 2015) and the interaction of TERMINATING FLOWER with *SlBOPs* to repress meristematic maturation in tomato flowers (MacAlister et al., 2012; Xu et al., 2016). We further hypothesize that *SlBOP2* and a transcription factor interact to regulate organogenic potential in complex leaves. Specifically, perhaps the TF transcription factor binds to the upstream regulatory region of *SlBOP2* (Figure 8F). We suggest that both *TF and SlBOP2* function in suppressing meristematic properties of the margin during an early developmental window that gradually closes with leaf maturation, an idea consistent with the view of the marginal blastozone described by Hagemann (1970).

While our understanding of the recruitment of genetic regulators in a spatiotemporal context continues to increase, one of the more exciting questions still remains: is the marginal meristem evolutionarily derived from the SAM (Floyd and Bowman, 2010)? Ectopic adventitious SAMs have been shown to occur on leaves of functional knockouts of *CUP-SHAPED-COTYLEDONS2* (*CUC2*) and *CUC3* (Hibara et al., 2003; Blein et al., 2008; Aichinger et al., 2012) and of Arabidopsis lines overexpressing homeobox genes *KNOTTED-1* (*KN1*) and *Kn1-like* (*KNAT1*; Sinha and Hake, 1994; Chuck et al., 1996) in a region analogous to the base of an emerging leaflet, suggesting developmental analogy and possibly homology to axillary meristems. Axillary meristems form on the adaxial surface at the boundary zone between the leaf and SAM, where BOP2 has already been shown to play a regulatory role in this process in tomato (Izhaki et al., 2018), barley (*Hordeum vulgare*; Tavakol et al., 2015; Dong et al., 2017), and maize (Dong et al., 2017). The ectopic meristem phenotype of *CR-slbop2* on the margins of complex tomato leaves suggests that signals might be recruited in the margin that are similar to those present in leaf initiation sites during axillary meristem formation. Our findings add further evidence that the margin is analogous, and possibly homologous at the process level, to the SAM. The leaf margin likely evolved via the genetic recruitment of similar regulatory factors, including BOP, reinforcing the importance of the reiteration of genetic mechanisms to establish distinct spatial identities in neighboring domains during plant development.

Our current understanding of the leaf margin is based on foundational work that defined the margin by explicitly tracking developmental landmarks (Avery, 1933; Poethig and Sussex, 1985a; Wolf et al., 1986; Dolan and Poethig, 1998). Early literature defined the leaf primordium as broadly meristematic during early development, with this meristematic potential becoming restricted and gradually lost as the leaf develops (Foster, 1936; Sachs, 1969; Hagemann and Gleissberg, 1996). Although such studies provide a roadmap for describing growth patterns in the margin, a major challenge is to understand how these patterns are specified at the genetic level (Coen et al., 2017; Whitewoods and Coen, 2017) and how this fits with our interpretation of the recruitment of regulatory mechanisms suppressing the morphogenetic potential of the margin during the evolution of leaves in seed plants. Plant development is reliant on reiterative patterning, and leaf development is no exception. Our findings suggest that we can describe leaf development as the reiteration and modulation of similar evolutionarily derived genetic programs that act to suppress the morphogenetic and organogenetic potential of meristematic regions in order to achieve final leaf form. Follow-up studies in additional species are needed to understand these evolutionarily conserved mechanisms and how they have been modulated to sculpt the diversity of leaf forms observed in nature.

Methods

Plant growth and tissue embedding

Seeds of tomato mutant *tf-2* (LA0512) and wild-type line Condine Red (LA0533) were obtained from the Tomato Genetics Resource Center. The seeds were sterilized with 50% bleach for two minutes and rinsed 10 times with distilled water. The seeds were placed on moist paper towels in Phytotrays (Sigma-Aldrich), incubated in the dark for 2 days, and allowed to germinate in a walk in Conviron growth chamber for 4 days before being transferred to soil (Sunshine Mix #1, Sun Gro Horticulture) for 8 days of growth; the seedlings were grown for a total of 14 days. Chambers were set for 16:8 light–dark cycle, with lighting consisting of alternating fluorescent (F48T12CWHO) 4050 Lumens bulbs. Generation of the transgenic DR5:Venus (cv. M82) line was described in (Shani et al., 2010) and the AtpPIN1:PIN1-GFP (cv. Moneymaker) line was described in (Bayer et al., 2009).

CR-bop-2 RNAi lines were received from the Lippman Lab at Cold Spring Harbor. CR-bop-2 RNAi and wild-type plant (M82) were germinated and grown in growth chambers for 2 weeks following methods above. Plants were further grown in a growth chamber for 1 month. After 1 month, plants were transferred to a greenhouse and grown under normal light conditions. The plants were observed, and any abnormalities were noted, dated, and photographed throughout the lifetime of each plant. The images are taken from mature leaves from plants that were 63 days old. Leaf complexity counts (Supplemental Figure 6) were taken at the age of 45 days old.

Plants were collected in the afternoon, vacuum infiltrated for 1 h with ice-cold 3:1 (100% EtOH: 100% acetic acid) fixative, and fixed overnight at 4°C. The samples were washed three times in 75% EtOH, passed through an EtOH series on a shaker at room temperature for 1 h per step (75, 85, 95, 100, 100, 100%), and incubated in 100% EtOH overnight at 4°C. All ethanol solutions were made using 2× autoclaved diethylpyrocarbonate (DEPC) treated water. The tissue was passed through a xylene/EtOH series for 2 h per step (25, 50, 75, 100, 100%) on a shaker at room temperature. The tissue was incubated overnight at room temperature in 100% xylene with 20–40 paraffin chips (Paraplast x-tra, Thermo Fisher Scientific), followed by incubation at 42°C until the paraffin dissolved. The paraffin:xylene solution was subsequently removed and replaced with 100% paraffin and the sample was incubated for 3 days at 55°C, with the solution changed twice daily. The tissue was then embedded using tools and surfaces that had been washed with RNAseZap (Thermo Fisher Scientific) and DEPC. The embedded blocks were transversely sectioned at 5- to 7-µm thickness using a Leica RM2125RT rotary microtome (Leica Microsystems) on RNase-free polyethylene naphthalate PEN membrane slides (Leica). The slides were dried at room temperature and deparaffinized with 100% xylene.

EdU visualization

Cell division was visualized by observing fluorescent signals derived from an EdU incorporation assay in which EdU is incorporated into cells during the S-phase (Kotogány et al., 2010). The EdU assay was performed as previously described (Ichihashi et al., 2011; Nakayama et al., 2014) with some modifications using a Click-iT EdU Alexa Fluor Imaging kit (Invitrogen). Fourteen-day-old seedlings were dissected under a microscope. After removing older leaves, P4 leaf epidermis was nicked using an insect mounting needle to increase infiltration in subsequent steps. The plant apex was incubated in water containing 10 µM EdU for 2 h. The samples were washed in 1× phosphate-buffered saline solution (PBS, pH 7.4) and fixed in Formaldehyde Alcohol Acetic Acid (FAA) under vacuum infiltration for 3 h. Subsequently, the samples were fixed in 3.7% formaldehyde in PBS (pH 7.4) for 30 min and washed three times in PBS with shaking. Alexa Fluor coupling to EdU was performed in the dark following the manufacturer's instructions. Photographs were taken under a Zeiss LSM 710 Confocal Microscope with excitation wavelengths set at 488 and 420 nm.

Flow cytometry and GUS staining

Ploidy levels were measured using a PA-I ploidy analyzer (Partec) as described previously (Sugimoto-Shirasu et al., 2002). We grew up 50 plants and sampled the oldest two leaves on the plant at each time point. To identify the leaves by counting from youngest leaves requires apical meristem destruction; therefore, we choose to measure leaf age from oldest leaf to youngest—Leaf 1 corresponds to the oldest leaf, Leaf 2 is second oldest, and so on. For the first two time points (Days 8 and 18), we sampled L1 or L2 and for the later time points, Day 30 and above, we sampled the oldest intact leaf, which because of age was often damaged, therefore the leaves sampled ranged from Leaf 2 to Leaf 5. All leaves sampled beyond Day 30 had reached maturity. Fresh tissue was extracted from whole leaves at the youngest leaf age (Day 8), whereas older stage tissue was extracted from both the top and bottom sections of the leaf (Days 18 to 90). The tissue was chopped with a razor blade. Cystain extraction buffer (Partec) was used to release nuclei. The solution was filtered through a CellTrics filter (Partec) and stained with Cystain fluorescent buffer (Partec). At least 4,000 nuclei isolated were used for each ploidy measurement. Flow cytometry experiments were repeated at least three times using independent biological replicates.

Histochemical localization of GUS activity was performed as previously described (Kang and Dengler, 2002). Representative images were chosen from >15 samples stained in 3 independent experiments.

Laser capture microdissection and RNA processing

Each tissue type was independently captured through serial sections using a Leica LMD6000 Laser Microdissection System (Leica Microsystems). Each biological replicate contained tissue collected from five to eight apices. Supplemental Figure 1 and Supplemental Movie 1 show how tissue regions were identified and dissected. Tissue was collected in lysis buffer from an RNAqueous-Micro Total RNA Isolation Kit (Ambion) and immediately stored at

−80°C. RNA extraction was performed using an RNAqueous-Micro Total RNA Isolation Kit (Ambion) following the manufacturer's instructions. The RNA was amplified using the WT-Ovation Pico RNA Amplification System (ver. 1.0, NuGEN Technologies Inc.). The RNA was purified using RNAClean magnetic beads (Agencourt) and processed within one month of fixation to ensure RNA quality.

RNA-seq libraries were created as described by Kumar and coworkers (Kumar et al., 2012), starting with the second-strand synthesis step, with the following modifications: For second-strand synthesis, 10 μL of cDNA (>250 ng) was combined with 0.5 μL of random primers and 0.5 μL of dNTP. The sample was incubated at 80°C for 2 min, followed by 60°C for 10 s, 50°C for 10 s, 40°C for 10 s, 30°C for 10 s, and 4°C for at least 2–5 min. After adding 5 μL of 10× DNA pol buffer, 31-μL water, and 2.5-μL DNA Pol I on ice, the sample was incubated at 16°C for 2.5 h. The process was continued following the published (Kumar et al., 2012) protocol starting with step 2.3: Bead purification of double-stranded DNA. The libraries were quality checked and quantified using a Bioanalyzer 2100 (Agilent) on RNA 6000 Pico Kit (Agilent) chips at the UC Davis Genome Center. The libraries were sequenced in three lanes using the HiSeq2000 Illumina Sequencer at the Vincent J Coates Genomics Sequencing Laboratory at UC Berkeley.

Read processing, differential expression, and GO enrichment analysis

Quality filtering, N removal, and adaptor trimming were performed on data from each of the three Illumina sequencing lanes separately. We first performed N removal using read_N_remover.py. Sequences below a quality (phred) score of 20 were removed without reducing the read size to below 35 bp. To remove adapter contamination, we used adapterEffectRemover.py, setting the minimum read length to 41. To assess the quality of the reads after pre-processing, we ran FASTQC (available at http://www.bioinformatics.bbsrc.ac.uk/projects/fastqc/) before and after pre-processing. To filter out reads from chloroplast or mitochondrial sequences, all libraries were mapped to the S.lycopersicum_AFYB01.1 mitochondrial sequence from NCBI and the NC_007898.3 chloroplast sequence from NCBI using STAR 2.4.0 (Dobin et al., 2013). Reads that did not map to either organelle were mapped to the ITAG3.10 *Solanum lycopersicum* genome using STAR 2.4.0, where nongenic sequences were masked using the inverse coordinates of the ITAG3.10 gene model gff file. Bedtools (Quinlan, 2014) coverageBed was then used to count mapped reads, using a bed file generated from ITAG3.10 gene models. We built an online visualization tool for the community to manually explore the reads generated across the six tissue types in both wild-type and *tf-2*: http://bar.utoronto.ca/efp_tomato/cgi-bin/efpWeb.cgi?dataSource=Tomato_Meristem (Winter et al., 2007; Patel et al., 2012).

Read processing and differential expression analyses were performed using the R package edgeR (Robinson et al., 2010). Pairwise differential gene expression in each region along the proximal–distal axis was calculated in each proximal–distal region (top, middle, base) in separate analyses. Differential gene expression was determined using the 'exactTest()' function in R (R Core Team, 2018), multiple testing correction was performed using the Benjamini–Hochberg procedure, and significance of differential expression was determined using a cutoff of FDR <0.05. To estimate differential expression of genes across the entire marginal blastozone and rachis regions, we used an additive linear model where the proximal–distal axis was assigned as a blocking factor, which adjusts for differences between the margin and rachis in the top, middle, and base: model.matrix (~Region + Tissue; Supplemental Data Set 3). For both pairwise and modeling analysis of differential expression, counts per million were calculated from raw reads, and genes with more than five reads in two or more reps were removed. We estimated common negative binomial dispersion and normalized counts across all samples using the trimmed mean of M-value method (Robinson and Oshlack, 2010). Normalized Read counts, as calculated by counts per million (c.p.m.), are available in Supplemental Data Set 9. GO enrichment analysis was performed using the R libraries GO.seq and GO.db (Supplemental Data Set 2). The GO terms were summarized further using REduce and VIsualize Gene Onology (REVIGO; http://revigo.irb.hr/) for Figure 3. The full code used for these analyses is available at https://github.com/iamciera/lcmProject.

SOM clustering

To explore the genes whose expression levels were the most variable across tissues, we identified the top 25% genes based on coefficient of variation and ratio of standard deviation compared with mean from our count data. To remove differences in counts between samples, the magnitude of gene expression data was scaled between 2 and -2 in wild-type and *tf-2* separately using the "scale()" function in R (R Core Team, 2018). Hexagonal layout was used for all SOM clustering (Kohonen). For basic SOM analysis, the SOM() function was used for each genotype separately, while superSOMs were performed using superSOM() in the Kohonen R package (Wehrens and Buydens, 2007; Wehrens and Kruisselbrink, 2018). Training for both methods was performed in 100 iterations in which the adaptive learning rate decreased from 0.05 to 0.01. Codebook vectors and distance plots of cluster assignments were generated using the visualization functions in ggplot2 (Wickham, 2009) and the Kohonen R package. To ensure that the major variances in gene expression patterns were defined by SOM clustering and to verify consistency in clustering, cluster assignments were projects onto the PC space. All scripts used in clustering are available at https://github.com/iamciera/lcmProject.

Supplemental data

The following materials are available in the online version of this article.

Supplemental Movie S1. Laser capture microdissection procedure.

Supplemental Figure S1. Rules for tissue collection via laser capture microdissection.

Supplemental Figure S2. Laser cutting to obtain sufficient amounts of RNA for RNA amplification and Illumina sequencing.

Supplemental Figure S3. Summary of the results of differential gene expression analysis in wild-type and *tf-2*.

Supplemental Figure S4. Relationship between SOM clustering analysis and PCA analysis performed on wild-type genes across tissues.

Supplemental Figure S5. Visualization of large SOM clustering analysis.

Supplemental Figure S6. Phenotyping of CR-slbop2 and genomic map of SlBOP2.

Supplemental Data Set S1. Results of differential gene expression analysis between the margin and rachis in the top, middle, and base regions of both genotypes (WT and *tf-2*).

Supplemental Data Set S2. GO terms describing differentially expressed genes between the margin and rachis in the top, middle, and base regions of both genotypes (WT and *tf-2*).

Supplemental Data Set S3. Results of differential expression analysis across the margin and rachis tissues performed with only wild-type reads and adjusted for variability between the proximal–distal axis.

Supplemental Data Set S4. Results from wild-type GO enrichment analysis to compare margin and rachis tissue and adjusted for variability between the proximal–distal axis.

Supplemental Data Set S5. Genes with the most variable expression.

Supplemental Data Set S6. SOM cluster assignments for wild type using a codemap vector of six showing the top six gene expression clusters.

Supplemental Data Set S7. GO terms derived from Data Set 6.

Supplemental Data Set S8. SOM cluster analysis using a codemap vector of 36 in wild-type.

Supplemental Data Set S9. Normalized Read counts calculated as c.p.m.

Supplemental Data Set S10. Results of differential expression analysis across the margin and rachis tissue performed with only *tf-2* reads and adjusted for variability between the proximal–distal axis.

Acknowledgments

The UC Davis Tomato Genetics Resource Center provided tomato germplasm. The AtpPIN1: PIN1: GFP and the DR5: VENUSx6 lines were gifts from Cris Kuhlemeier (University of Bern) and Naomi Ori (Hebrew University, Israel), respectively. We thank Zachary Lippman (Cold Spring Harbor Laboratory) for the *CR-slbop2* lines. We would also like to acknowledge Eddi Esteban, Asher Pasha, and Nicholas J. Provart for building the EFP browser. We thank Daniel Chitwood (Michigan State University) who provided computational training and insightful discussion, which greatly facilitated the research and Kristina Zumstein (UC Davis) for her work and organization on several experiments. We would also like to thank Siobhan Brady (UC Davis) and Andrew Groover (USDA) for their helpful comments and John Harada (UC Davis) and Julie Pelletier (UC Davis) for use and training on the laser capture microdissection microscope.

Funding

C.C.M. was supported by a National Science Foundation Graduate Research Fellowship (grant no. DGE-1148897), Katherine Esau Summer Fellowship, Walter R. and Roselinde H. Russell Fellowship, and Elsie Taylor Stocking Fellowship. C.C.M. holds a Postdoctoral Enrichment Program Award from the Burroughs Wellcome Fund. Part of this work was supported by National Science Foundation (NSF) PGRP grant IOS–0820854 (to N.R.S., Julin Maloof and Jie Peng), NSF grant IOS-1558900 to N.R.S., and S.L was partially supported by IOS 1856749 (to Julia Bailey-Serres, Siobhan Brady, Roger Deal, Uta Paszcowsky, and N.R.S.). C.C.M. was also supported by a collaboration between the National Science Foundation and the Japan Society for the Promotion of Science with a Graduate Research Opportunities Worldwide award. This material utilized resources supported by the National Science Foundation under Award Numbers DBI-0735191, DBI-1265383, and DBI-1743442. URL: www.cyverse.org.

Conflict of interest statement. None declared.

References

Abraham Juárez MJ, Hernández Cárdenas R, Santoyo Villa JN, O'Connor D, Sluis A, Hake S, Ordaz-Ortiz J, Terry L, Simpson J (2015) Functionally different PIN proteins control auxin flux during bulbil development in Agave tequilana. J Exp Bot **66**: 3893–3905

Aichinger E, Kornet N, Friedrich T, Laux T (2012) Plant stem cell niches. Annu Rev Plant Biol **63**: 615–636

Andriankaja M, Dhondt S, De Bodt S, Vanhaeren H, Coppens F, De Milde L, Mühlenbock P, Skirycz A, Gonzalez N, Beemster GTS et al. (2012) Exit from proliferation during leaf development in Arabidopsis thaliana: a not-so-gradual process. Dev Cell **22**: 64–78

Avery GS (1933) Structure and development of the tobacco leaf. Am J Bot **20**: 565–592

Bayer EM, Smith RS, Mandel T, Nakayama N, Sauer M, Prusinkiewicz P, Kuhlemeier C (2009) Integration of transport-based models for phyllotaxis and midvein formation. Genes Dev **23**: 373–384

Beemster GTS, De Veylder L, Vercruysse S, West G, Rombaut D, Van Hummelen P, Galichet A, Gruissem W, Inzé D, Vuylsteke M (2005) Genome-wide analysis of gene expression profiles associated with cell cycle transitions in growing organs of Arabidopsis. Plant Physiol **138**: 734–743

Bendahmane A,Theres K (2011) Shoot branching and leaf dissection in tomato are regulated by homologous gene modules. Plant Cell 1–16 http://www.plantcell.org/content/23/10/3595.short

Benková E, Michniewicz M, Sauer M, Teichmann T, Seifertová D, Jürgens G, Friml J (2003) Local, efflux-dependent auxin gradients as a common module for plant organ formation. Cell **115**: 591–602

Bennett T, Brockington SF, Rothfels C, Graham S, Stevenson D, Kutchan T, Rolf M, Thomas P, Wong GK-S, Leyser O et al.

(2014) Paralagous radiations of PIN proteins with multiple origins of non-canonical PIN structure. Mol Biol Evol **31**: 2042–2060

Bergervoet JHW, Berhoeven HA, Gilissen LJW, Bino RJ (1996) High amounts of nuclear DNA in tomato (*Lycopersicon esculentum* Mill.) pericarp. Plant Sci **116**: 141–145

Bilsborough GD, Runions A, Barkoulas M, Jenkins HW, Hasson A, Galinha C, Laufs P, Hay A, Prusinkiewicz P, Tsiantis M (2011) Model for the regulation of Arabidopsis thaliana leaf margin development. Proc Natl Acad Sci USA **108**: 3424–3429

Bläsing OE, Gibon Y, Günther M, Höhne M, Morcuende R, Osuna D, Thimm O, Usadel B, Scheible W-R, Stitt M (2005) Sugars and circadian regulation make major contributions to the global regulation of diurnal gene expression in Arabidopsis. Plant Cell **17**: 3257–3281

Blein T, Pulido A, Vialette-Guiraud A, Nikovics K, Morin H, Hay A, Johansen IE, Tsiantis M, Laufs P (2008) A conserved molecular framework for compound leaf development. Science **322**: 1835–1839

Bourdon M, Frangne N, Mathieu-Rivet E, Nafati M, Cheniclet C, Renaudin J-P, Chevalier C (2010) Endoreduplication and Growth of Fleshy Fruits. In U Lüttge, W Beyschlag, B Büdel, D Francis, eds, Progress in Botany, Vol. **71**, Progress in Botany, Springer, Berlin, Germany, pp. 101–132

Cheniclet C, Rong WY, Causse M, Frangne N, Bolling L, Carde J-P, Renaudin J-P (2005) Cell expansion and endoreduplication show a large genetic variability in pericarp and contribute strongly to tomato fruit growth. Plant Physiol **139**: 1984–1994

Chuck G, Lincoln C, Hake S (1996) KNAT1 induces lobed leaves with ectopic meristems when overexpressed in Arabidopsis. Plant Cell **8**: 1277–1289

Coen E, Kennaway R, Whitewoods C (2017) On genes and form. Development **144**: 4203–4213

De Veylder L, Larkin JC, Schnittger A (2011) Molecular control and function of endoreplication in development and physiology. Trends Plant Sci **16**: 624–634

Dobin A, Davis CA, Schlesinger F, Drenkow J, Zaleski C, Jha S, Batut P, Chaisson M, Gingeras TR (2013) STAR: ultrafast universal RNA-seq aligner. Bioinformatics **29**: 15–21

Dolan L, Poethig R (1998) Clonal analysis of leaf development in cotton. Am J Bot **85**: 315

Dong Z, Li W, Unger-Wallace E, Yang J, Vollbrecht E, Chuck G (2017) Ideal crop plant architecture is mediated by tassels replace upper ears1, a BTB/POZ ankyrin repeat gene directly targeted by TEOSINTE BRANCHED1. Proc Natl Acad Sci USA **114**: E8656–E8664

Donnelly PM, Bonetta D, Tsukaya H, Dengler RE, Dengler NG (1999) Cell cycling and cell enlargement in developing leaves of Arabidopsis. Dev Biol **215**: 407–419

Efroni I, Blum E, Goldshmidt A, Eshed Y (2008) A protracted and dynamic maturation schedule underlies Arabidopsis leaf development. Plant Cell **20**: 2293–2306

Eshed Y, Baum SF, Perea JV, Bowman JL (2001) Establishment of polarity in lateral organs of plants. Curr Biol **11**: 1251–1260

Floyd SK,Bowman JL (2010) Gene expression patterns in seed plant shoot meristems and leaves: homoplasy or homology? J Plant Res **123**: 43–55

Foster AS (1936) Leaf differentiation in angiosperms. Bot Rev **2**: 349–372

Francis D, Halford NG (2006) Nutrient sensing in plant meristems. Plant Mol Biol **60**: 981–993

Gutierrez C (2005) Coupling cell proliferation and development in plants. Nat Cell Biol **7**: 535–541

Ha CM, Jun JH, Nam HG, Fletcher JC (2004) BLADE-ON-PETIOLE1 encodes a BTB/POZ domain protein required for leaf morphogenesis in *Arabidopsis thaliana*. Plant Cell Physiol **45**: 1361–1370

Ha CM, Kim G-T, Kim BC, Jun JH, Soh MS, Ueno Y, Machida Y, Tsukaya H, Nam HG (2003) The BLADE-ON-PETIOLE 1 gene controls leaf pattern formation through the modulation of meristematic activity in Arabidopsis. Development **130**: 161–172

Hagemann W,Gleissberg S (1996) Organogenetic capacity of leaves: The significance of marginal blastozones in angiosperms. Plant Syst Evol **199**: 121–152

Hay A, Tsiantis M (2006) The genetic basis for differences in leaf form between Arabidopsis thaliana and its wild relative *Cardamine hirsuta*. Nat Genet **38**: 942–947

Heisler MG, Ohno C, Das P, Sieber P, Reddy GV, Long JA, Meyerowitz EM (2005) Patterns of auxin transport and gene expression during primordium development revealed by live imaging of the Arabidopsis inflorescence meristem. Curr Biol **15**: 1899–1911

Hepworth SR, Pautot VA (2015) Beyond the divide: boundaries for patterning and stem cell regulation in plants. Front Plant Sci **6**: 1052

Hibara K-I, Takada S, Tasaka M (2003) CUC1 gene activates the expression of SAM-related genes to induce adventitious shoot formation. Plant J **36**: 687–696

Ichihashi Y, Kawade K, Usami T, Horiguchi G, Takahashi T, Tsukaya H (2011) Key proliferative activity in the junction between the leaf blade and leaf petiole of Arabidopsis. Plant Physiol **157**: 1151–1162

Ichihashi Y, Aguilar-Martínez JA, Farhi M, Chitwood DH, Kumar R, Millon LV, Peng J, Maloof JN, Sinha NR (2014) Evolutionary developmental transcriptomics reveals a gene network module regulating interspecific diversity in plant leaf shape. Proc Natl Acad Sci USA **111**: E2616–E2621

Izhaki A, Alvarez JP, Cinnamon Y, Genin O, Liberman-Aloni R, Eyal Y (2018) The tomato BLADE ON PETIOLE and TERMINATING FLOWER regulate leaf axil patterning along the proximal-distal axes. Front Plant Sci **9**: 1126

Joubès J, Chevalier C, Dudits D, Heberle-Bors E, Inzé D, Umeda M, Renaudin J-P (2000) CDK-related protein kinases in plants. In D Inzé, ed, The Plant Cell Cycle, Springer, the Netherlands, pp. 63–76

Kang J,Dengler N (2002) Cell cycling frequency and expression of the homeobox gene ATHB-8 during leaf vein development in Arabidopsis. Planta **216**: 212–219

Kawamura E, Horiguchi G, Tsukaya H (2010) Mechanisms of leaf tooth formation in Arabidopsis. Plant J **62**: 429–441

Kende H, Bradford K, Brummell D, Cho HT, Cosgrove D, Fleming A, Gehring C, Lee Y, McQueen-Mason S, Rose J, Voesenek LACJ (2004) Nomenclature for members of the expansin superfamily of genes and proteins. Plant Mol Biol **55**: 311–314. 10.1007/s11103-004-0158-6

Kidner CA, Timmermans MCP (2007) Mixing and matching pathways in leaf polarity. Curr Opin Plant Biol **10**: 13–20

Koenig D, Bayer E, Kang J, Kuhlemeier C, Sinha N (2009) Auxin patterns *Solanum lycopersicum* leaf morphogenesis. Development **136**: 2997–3006

Kohonen T (1982) Self-organized formation of topologically correct feature maps. Biol Cybern **43**: 59–69

Kondorosi E, Roudier F, Gendreau E (2000) Plant cell-size control: growing by ploidy? Curr Opin Plant Biol **3**: 488–492

Kotogány E, Dudits D, Horváth GV, Ayaydin F (2010) A rapid and robust assay for detection of S-phase cell cycle progression in plant cells and tissues by using ethynyl deoxyuridine. Plant Methods **6**: 5

Kumar R, Ichihashi Y, Kimura S, Chitwood DH, Headland LR, Peng J, Maloof JN, Sinha NR (2012) A high-throughput method for illumina RNA-Seq library preparation. Front Plant Sci **3**: 202

Hülskamp M, Misŕa S, Jürgens G (1994) Genetic dissection of trichome cell development in Arabidopsis. Cell **76**: 555–566

Lastdrager J, Hanson J, Smeekens S (2014) Sugar signals and the control of plant growth and development. J Exp Bot **65**: 799–807

Lilley JLS, Gee CW, Sairanen I, Ljung K, Nemhauser JL (2012) An endogenous carbon-sensing pathway triggers increased auxin flux and hypocotyl elongation. Plant Physiol **160**: 2261–2270

Li P, Ponnala L, Gandotra N, Wang L, Si Y, Tausta SL, Kebrom TH, Provart N, Patel R, Myers CR, et al. (2010) The developmental dynamics of the maize leaf transcriptome. Nat Genet **42**: 1060–1067

Liu X-D,Shen Y-G (2004) NaCl-induced phosphorylation of light harvesting chlorophyll a/b proteins in thylakoid membranes from the halotolerant green alga, Dunaliella salina. FEBS Lett **569**: 337–340

Ljung K (2013) Auxin metabolism and homeostasis during plant development. Development **140**: 943–950

MacAlister CA, Park SJ, Jiang K, Marcel F, Bendahmane A, Izkovich Y, Eshed Y, Lippman ZB (2012) Synchronization of the flowering transition by the tomato TERMINATING FLOWER gene. Nat Genet **44**: 1393–1398

Martinez CC, Koenig D, Chitwood DH, Sinha NR (2016) A sister of PIN1 gene in tomato (*Solanum lycopersicum*) defines leaf and flower organ initiation patterns by maintaining epidermal auxin flux. Dev Biol **419**: 85–98

Melaragno JE, Mehrotra B, Coleman AW (1993) Relationship between endopolyploidy and cell size in epidermal tissue of Arabidopsis. Plant Cell **5**: 1661–1668

Mitra A, Han J, Zhang ZJ, Mitra A (2009) The intergenic region of Arabidopsis thaliana cab1 and cab2 divergent genes functions as a bidirectional promoter. Planta **229**: 1015–1022

Moon J,Hake S (2011) How a leaf gets its shape. Curr Opin Plant Biol **14**: 24–30

Nakayama H, Nakayama N, Seiki S, Kojima M, Sakakibara H, Sinha N, Kimura S (2014) Regulation of the KNOX-GA gene module induces heterophyllic alteration in North American lake cress. Plant Cell **26**: 4733–4748

Naz AA, Raman S, Martinez CC, Sinha NR, Schmitz G, Theres K (2013) Trifoliate encodes an MYB transcription factor that modulates leaf and shoot architecture in tomato. Proc Natl Acad Sci USA **110**: 2401–2406

Nishio S, Moriguchi R, Ikeda H, Takahashi H, Takahashi H, Fujii N, Guilfoyle TJ, Kanahama K, Kanayama Y (2010) Expression analysis of the auxin efflux carrier family in tomato fruit development. Planta **232**: 755–764

O'Connor DL, Runions A, Sluis A, Bragg J, Vogel JP, Prusinkiewicz P, Hake S (2014) A division in PIN-mediated auxin patterning during organ initiation in grasses. PLoS Comput Biol **10**: e1003447

Ori N et al. (2007) Regulation of LANCEOLATE by miR319 is required for compound-leaf development in tomato. Nat Genet **39**: 787–791

Osuna D, Usadel B, Morcuende R, Gibon Y, Bläsing OE, Höhne M, Günter M, Kamlage B, Trethewey R, Scheible W-R et al. (2007) Temporal responses of transcripts, enzyme activities and metabolites after adding sucrose to carbon-deprived Arabidopsis seedlings. Plant J **49**: 463–491

Patel RV, Nahal HK, Breit R, Provart NJ (2012) BAR expressolog identification: expression profile similarity ranking of homologous genes in plant species. Plant J **71**: 1038–1050

Pattison RJ,Catalá C (2012) Evaluating auxin distribution in tomato (Solanum lycopersicum) through an analysis of the PIN and AUX/LAX gene families. Plant J **70**: 585–598

Pijnacker LP, Sree Ramulu K, Dijkhuis P, Ferwerda MA (1989) Flow cytometric and karyological analysis of polysomaty and polyploidization during callus formation from leaf segments of various potato genotypes. Theor Appl Genet **77**: 102–110

Poethig RS,Sussex IM (1985a) The cellular parameters of leaf development in tobacco: a clonal analysis. Planta **165**: 170–184

Poethig RS,Sussex IM (1985b) The developmental morphology and growth dynamics of the tobacco leaf. Planta **165**: 158–169

Price J, Laxmi A, St Martin SK, Jang J-C (2004) Global transcription profiling reveals multiple sugar signal transduction mechanisms in Arabidopsis. Plant Cell **16**: 2128–2150

Quinlan AR (2014) BEDTools: the Swiss-army tool for genome feature analysis. Curr Protoc Bioinformatics **47**: 11–12

Core Team R (2018) R: A language and environment for statistical computing. R Foundation for Statistical Computing, Vienna, Austria

Reinhardt D, Pesce E-R, Stieger P, Mandel T, Baltensperger K, Bennett M, Traas J, Friml J, Kuhlemeier C (2003) Regulation of phyllotaxis by polar auxin transport. Nature **426**: 255–260

Riou-Khamlichi C, Menges M, Healy JM, Murray JA (2000) Sugar control of the plant cell cycle: differential regulation of Arabidopsis D-type cyclin gene expression. Mol Cell Biol **20**: 4513–4521

Robinson R, Rick CM (1954) New tomato seedling characters and their linkage relationships. J Hered **45**: 241–248

Robinson MD, McCarthy DJ, Smyth GK (2010) edgeR: a Bioconductor package for differential expression analysis of digital gene expression data. Bioinformatics **26**: 139–140

Robinson MD,Oshlack A (2010) A scaling normalization method for differential expression analysis of RNA-seq data. Genome Biol **11**: R25

Sachs T (1969) Regeneration experiments on the determination of the form of leaves. Israel J Bot **18**: 21–30

Sairanen I, Novák O, Pěnčík A, Ikeda Y, Jones B, Sandberg G, Ljung K (2012) Soluble carbohydrates regulate auxin biosynthesis via PIF proteins in Arabidopsis. Plant Cell **24**: 4907–4916

Scarpella E, Barkoulas M, Tsiantis M (2010) Control of leaf and vein development by auxin. Cold Spring Harb Perspect Biol **2**: a001511

Scarpella E,Helariutta Y (2010) Vascular pattern formation in plants. Curr Top Dev Biol **91**: 221–265

Scarpella E, Marcos D, Friml J, Berleth T (2006) Control of leaf vascular patterning by polar auxin transport. Genes Dev **20**: 1015–1027

Shani E, Ben-Gera H, Shleizer-Burko S, Burko Y, Weiss D, Ori N (2010) Cytokinin regulates compound leaf development in tomato. Plant Cell **22**: 3206–3217

Sinha N,Hake S (1994) The Knotted leaf blade is a mosaic of blade, sheath, and auricle identities. Dev Genet **15**: 401–414

Skirycz A, Claeys H, De Bodt S, Oikawa A, Shinoda S, Andriankaja M, Maleux K, Eloy NB, Coppens F, Yoo S-D et al. (2011) Pause-and-stop: the effects of osmotic stress on cell proliferation during early leaf development in Arabidopsis and a role for ethylene signaling in cell cycle arrest. Plant Cell **23**: 1876–1888

Stokes ME, Chattopadhyay A, Wilkins O, Nambara E, Campbell MM (2013) Interplay between sucrose and folate modulates auxin signaling in Arabidopsis. Plant Physiol **162**: 1552–1565

Sugimoto-Shirasu K,Roberts K (2003) "Big it up": endoreduplication and cell-size control in plants. Curr Opin Plant Biol **6**: 544–553

Sugimoto-Shirasu K, Stacey NJ, Corsar J, Roberts K, McCann MC (2002) DNA topoisomerase VI is essential for endoreduplication in Arabidopsis. Curr Biol **12**: 1782–1786

Sussex IM,Kerk NM (2001) The evolution of plant architecture. Curr Opin Plant Biol **4**: 33–37

Tamayo P, Slonim D, Mesirov J, Zhu Q, Kitareewan S, Dmitrovsky E, Lander ES, Golub TR (1999) Interpreting patterns of gene expression with self-organizing maps: methods and application to hematopoietic differentiation. Proc Natl Acad Sci USA **96**: 2907–2912

Tavakol E et al. (2015) The barley Uniculme4 gene encodes a BLADE-ON-PETIOLE-like protein that controls tillering and leaf patterning. Plant Physiol **168**: 164–174

Tian C, Wang Y, Yu H, He J, Wang J, Shi B, Du Q, Provart NJ, Meyerowitz EM, Jiao Y2019) A gene expression map of shoot domains reveals regulatory mechanisms. Nat Commun **10**: 141

Tindamanyire JM, Townsley B, Kiggundu A, Tushemereirwe W, Sinha N (2013) Building a bi-directional promoter binary vector from the intergenic region of Arabidopsis thaliana cab1 and cab2 divergent genes useful for plant transformation. Afr J Biotechnol **12**: 1203–1208

Tsukaya H (2014) Comparative leaf development in angiosperms. Curr Opin Plant Biol **17**: 103–109

Usadel B, Bläsing OE, Gibon Y, Retzlaff K, Höhne M, Günther M, Stitt M (2008) Global transcript levels respond to small changes of the carbon status during progressive exhaustion of carbohydrates in *Arabidopsis rosettes*. Plant Physiol **146**: 1834–1861

Wehrens R, Buydens L (2007) Self- and Super-organizing Maps in R: The kohonen Package. J Stat Softw **21**: 1–19

Wehrens R, Kruisselbrink J (2018) Flexible Self-Organizing Maps in Kohonen 3.0. J Stat Softw **87**: 1–18

Whitewoods CD, Coen E (2017) Growth and development of three-dimensional plant form. Curr Biol **27**: R910–R918

Wickham H (2009) ggplot2: Elegant Graphics for Data Analysis. Springer Science & Business Media, New York

Wind J, Smeekens S, Hanson J (2010) Sucrose: metabolite and signaling molecule. Phytochemistry **71**: 1610–1614

Winter D, Vinegar B, Nahal H, Ammar R, Wilson GV, Provart NJ (2007) An "electronic fluorescent pictograph" browser for exploring and analyzing large-scale biological data sets. PLoS One **2**: e718

Wolf SD, Silk WK, Plant RE (1986) Quantitative patterns of leaf expansion: comparison of normal and malformed leaf growth in *Vitis vinifera* cv. ruby red. Am J Bot **73**: 832–846

Xu C, Park SJ, Van Eck J, Lippman ZB (2016) Control of inflorescence architecture in tomato by BTB/POZ transcriptional regulators. Genes Dev **30**: 2048–2061

Yifhar T, Pekker I, Peled D, Friedlander G, Pistunov A, Sabban M, Wachsman G, Alvarez JP, Amsellem Z, Eshed Y (2012) Failure of the tomato trans-acting short interfering RNA program to regulate AUXIN RESPONSE FACTOR3 and ARF4 underlies the wiry leaf syndrome. Plant Cell **24**: 3575–3589